



OPEN

Inhibition of breast cancer growth and metastasis by a biomimetic peptide

SUBJECT AREAS:

TUMOUR
ANGIOGENESIS

BREAST CANCER

METASTASES

Esak Lee¹, Seung Jae Lee¹, Jacob E. Koskimaki¹, Zheyi Han¹, Niranjan B. Pandey¹ & Aleksander S. Popel^{1,2}¹Department of Biomedical Engineering, Johns Hopkins University School of Medicine, Baltimore, MD 21205, United States,²Department of Oncology and the Sidney Kimmel Comprehensive Cancer Center, Johns Hopkins University School of Medicine, Baltimore, MD 21231, United States.Received
24 June 2014Accepted
5 November 2014Published
20 November 2014Correspondence and
requests for materials
should be addressed to
A.S.P. (apopel@jhu.
edu)

Metastasis is the main cause of mortality in cancer patients. Though there are many anti-cancer drugs targeting primary tumor growth, anti-metastatic agents are rarely developed. Angiogenesis and lymphangiogenesis are crucial for cancer progression, particularly, lymphangiogenesis is pivotal for metastasis in breast cancer. Here we report that a novel collagen IV derived biomimetic peptide inhibits breast cancer growth and metastasis by blocking angiogenesis and lymphangiogenesis. The peptide inhibits blood and lymphatic endothelial cell viability, migration, adhesion, and tube formation by targeting IGF1R and Met signals. The peptide blocks MDA-MB-231 tumor growth by inhibiting tumor angiogenesis *in vivo*. Moreover, the peptide inhibits lymphangiogenesis in primary tumors. MDA-MB-231 tumor conditioned media (TCM) was employed to accelerate spontaneous metastasis in tumor xenografts, and the anti-metastatic activity of the peptide was tested in this model. The peptide prevents metastasis to the lungs and lymph nodes by inhibiting TCM-induced lymphangiogenesis and angiogenesis in the pre-metastatic organs. In summary, a novel biomimetic peptide inhibits breast cancer growth and metastasis by blocking angiogenesis and lymphangiogenesis in the pre-metastatic organs as well as primary tumors.

Breast cancer is the most frequently diagnosed malignancy among women in the United States¹. Although anti-angiogenic agents have been used for treating breast cancer in the clinic, overall survival in advanced breast cancer patients has not been substantially improved² possibly because breast cancer metastasis occurs preferentially via lymphatic dissemination compared to hematogenous spread³. Thus, there is an unmet need to develop therapeutic agents to block lymphangiogenesis as well as angiogenesis to efficiently block breast tumor growth and metastasis.

We have identified several endogenous peptides to inhibit lymphangiogenesis by using bioinformatics-aided methodologies and *in vitro* and animal experiments⁴⁻⁷. Lee et al. have reported that short peptides derived from somatotropin domain-containing proteins inhibit lymphatic endothelial cell (LEC) proliferation, migration, adhesion, and tube formation⁵. Lee et al. have also documented that a 14-mer peptide derived from transmembrane protein 45A (TMEM45A), a member of the somatotropin family of proteins, exhibits potent anti-lymphangiogenic activity in breast tumor xenografts and in tumor-conditioned lymph nodes⁴. Koskimaki et al. showed synergy between the collagen IV derived mimetic peptide SP2012 and the TMEM45A peptide as lymphangiogenesis inhibitors⁶. This collagen IV derived peptide has also shown potent anti-angiogenic activity in earlier studies^{6,8,9}. When tested separately, the collagen IV peptide SP2012 was significantly more potent than TMEM45A peptide in inhibition of angiogenesis; its activity was comparable to the TMEM45A peptide in inhibition of lymphangiogenesis⁶. Based on these findings, SP2012 was further optimized to be soluble, easy to synthesize and stable by using bioinformatics and amino acid mutation methodologies^{9,10}. Here we report the *in vitro* and *in vivo* activities of the optimized collagen IV biomimetic peptide SP2043, whose amino acid sequence is LRRFSTAPFAFIDINDVINP. This peptide has activity against lymphangiogenesis and angiogenesis, and inhibits the growth of a primary triple negative breast cancer (TNBC) tumor xenograft and its metastasis to the lungs and lymph nodes by blocking lymphangiogenesis and angiogenesis in pre-metastatic organs as well as primary tumors. For the metastasis study we employ a tumor-conditioned media (TCM) mediated spontaneous metastasis model developed previously in our laboratory^{11,12}, which shows accelerated formation of thoracic metastases within one month after orthotopic tumor inoculation into the inguinal mammary fat pad. The use of TCM mimics secretion of pro-metastatic factors by the primary tumor in patients.



Results

SP2043 blocks viability, adhesion, migration and tube formation of lymphatic and blood endothelial cells. The effect of SP2043 on cell viability, adhesion, migration, and tube formation of human

umbilical vein endothelial cells (HUVEC) was tested (Fig. 1a–e). The WST-1 reagent was used to determine the effect of SP2043 on the viability of HUVEC. SP2043 inhibits HUVEC viability with an IC_{50} value of $7.0 \pm 2.1 \mu\text{M}$ (Fig. 1a). The real time cell analysis

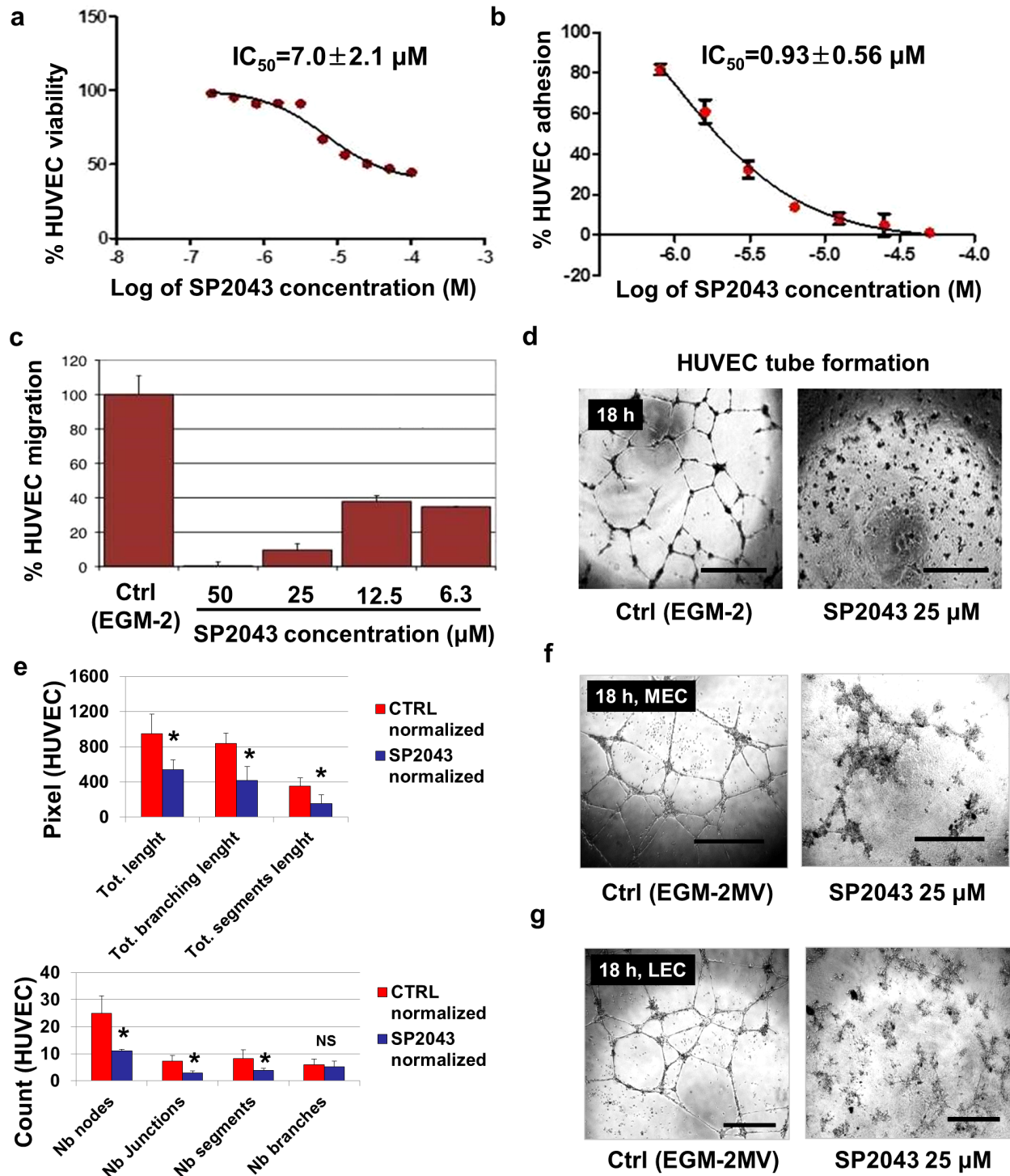


Figure 1 | In vitro activity of SP2043 on HUVEC, MEC, and LEC. SP2043 blocks angiogenesis and lymphangiogenesis in vitro. The controls for cell viability, migration, adhesion, and tube formation assays correspond to cell phenotypes in normal endothelial growth media (EGM-2 in the HUVEC experiment, or EGM-2MV in LEC and MEC experiments). (a) Inhibition of HUVEC viability. (b) Inhibition of HUVEC adhesion. (c) Inhibition of HUVEC migration. (d) Inhibition of HUVEC tube formation at 18 h. Scale bars represent 200 μm . (e) Quantification of (d). HUVEC tube formation was quantified by using Angiogenesis Analyzer for ImageJ (NIH). The process is described in the Supplementary Fig. S8 online and Methods. Briefly, the original images (3 images per group) were transformed to the skeletonized binary tree images. These were analyzed and all the values were normalized with the analyzed area. Number of nodes (Nb nodes), Nb junctions, Nb segments, Nb branches, total length (Tot length), Tot branching length, and Tot segment length were obtained (* $P < 0.05$). (f) Inhibition of MEC tube formation at 18 h. Scale bars represent 200 μm . (g) Inhibition of LEC tube formation at 18 h. Scale bars represent 200 μm . Data (a,b,e) are reported as mean \pm s.e.m.



(RTCA) system was employed to measure HUVEC adhesion and migration. The RTCA system (ACEA) measures electrical impedance. Gold electrodes embedded on the bottom of a 96-well plate to measure adhesion or on the underside of the top chamber of a Boyden-chamber-like 2-chamber setup to measure migration register the number of cells or the extent of contact between the cells and the electrodes as a change in impedance. This change is converted to a cell index that is a direct measure of the amount of adhesion or the number of migrated cells. SP2043 inhibits HUVEC adhesion (IC_{50} value of $0.93 \pm 0.56 \mu\text{M}$) and migration (IC_{50} value less than $6.3 \mu\text{M}$) (Fig. 1b,c). HUVEC tube formation is also blocked by SP2043 (Fig. 1d). Tube formation was analyzed by using Angiogenesis Analyzer for ImageJ (NIH). Number of nodes (Nb nodes), Number of junctions (Nb junctions), Number of segments (Nb segments), Number of branches (Nb branches), total length (Tot length), Tot branching length, and Tot segment length were obtained and normalized. The pixel number of the analyzed area is taken to be 100,000. From the analysis, we showed that SP2043 treatment inhibits HUVEC tube formation (Fig. 1e). HUVEC are routinely used in angiogenesis in vitro assays, but due to their venous origin they may not adequately represent tumor microvessels. For this reason we tested SP2043 on microvascular endothelial cells (MEC) which are derived from capillaries: SP2043 blocks MEC tube formation and adhesion (Fig. 1f and Supplementary Fig. S1 online). SP2043 also inhibits the adhesion and tube formation of lymphatic endothelial cells (LEC) (Fig. 1g and Supplementary Fig. S1 online).

Scrambled-SP2043 (Scram-2043; seq: LRRFSTAPFAFIPEAKVINP) was prepared by replacing “DIND” from the SP2043 (seq: LRRFSTAPFAFIDINDVINP) with “PEAK” (Supplementary Fig. S2 online). The detailed rationale for the preparation of this scrambled peptide is described in the Methods (‘Peptide synthesis and handling’). Scram-2043 inhibits MEC adhesion and migration very poorly compared to SP2043 showing that the scrambled peptide has lost most of activity compared to SP2043, and that the activity of SP2043 is amino acid sequence specific (Supplementary Fig. S2 online).

SP2043 blocks IGF1R and Met signals in lymphatic and blood endothelial cells. We previously found that the collagen IV biomimetic peptide SP2012, which is an earlier analog of SP2043, inhibits VEGFR2 signaling pathways in blood endothelial cells by interacting with $\beta 1$ integrin⁶⁸. As the $\beta 1$ integrin can associate with diverse receptor tyrosine kinase receptors, including VEGFR2, Met, IGF1R, and EGFR in diverse cell types, here we expand its molecular targets^{13–16}. We showed that EGF-induced phosphorylation of EGFR and its downstream signals (MAPK and Akt) are not blocked by SP2043 (Supplementary Fig. S3 online). Therefore, the effect of SP2043 on the IGF1R and Met signaling pathways in endothelial cells were further studied (Fig. 2). In HGF-induced MEC, SP2043 blocks the levels of phospho-Met (Y1234/1235/1349), phosph-Gab1 (Y307) and phospho-MAPK (T202/Y204) (Fig. 2a). In IGF1 induced MEC, SP2043 inhibits the level of phospho-IGF1R (Y1135/1136) and inhibits phosphorylation of MAPK and Akt (S473) (Fig. 2b). HGF induces the phosphorylation of Met and Akt in LEC. These phosphorylations are blocked by SP2043 in a dose dependent manner (Fig. 2c). SP2043 also blocks the phosphorylation of IGF1R, MAPK induced by IGF treatment of LEC (Fig. 2d).

CD58, CD155, and ADAM17 dissociate from IGF1R and Met receptor complexes upon SP2043 treatment. To understand the multimodal inhibition of the IGF1R and Met signals by the SP2043 peptide, first the protein components of the IGF1R or Met receptor complexes induced by IGF1 or HGF were determined. Next the proteins that were dissociated from the IGF1R or Met receptor complexes after SP2043 treatment were identified. In IGF1 induced MEC, 11 proteins are found to be part of the receptor complex with IGF1R (CD58, CD155, CD31, CD36, CD44, CD147,

RECK, ADAM17, Galectin-3, Integrin $\beta 1$, and Integrin $\beta 2$). After SP2043 treatment, 8 of these proteins (CD31, CD147, Integrin $\beta 1$, RECK, Galectin-3, CD58, CD155, ADAM17) are found to dissociate from the receptor complex (Fig. 3a). In HGF-induced MEC, 8 proteins are found to be part of the receptor complex with Met (CD58, CD155, TIMP3, CD36, CD154, CD44, ADAM17, Integrin $\beta 2$). After SP2043 treatment, 7 of these proteins (CD58, CD155, TIMP3, CD36, CD154, CD44, ADAM17) are found to dissociate from the receptor complex (Fig. 3b). Taken together, CD58, CD155, and ADAM17 are targeted by SP2043 and dissociated from both the IGF1R and Met receptor complexes (Fig. 3c).

SP2043 inhibits viability of MDA-MB-231, MCF-7, and SUM-149 breast cancer cells. The roles of IGF1R, Met, CD58, CD155, and ADAM17 in cancer progression have been studied^{17–21}. Given the role of the IGF and HGF signaling pathways in breast cancer cells^{22–25} and the result of inhibition of IGF1R and Met signals by the peptide and the dissociation of CD58, CD155, and ADAM17 from the IGF1R and Met receptor complexes, we hypothesized that the SP2043 peptide influences breast cancer cells as well. The potential anti-proliferative potential of SP2043 on breast cancer cells was tested on two triple-negative breast cancer (TNBC) cell lines (MDA-MB-231 and SUM-149), and one estrogen receptor-positive (ER+) breast cancer cell line (MCF-7). The peptide inhibits viability of MDA-MB-231 (IC_{50} value of $22.1 \pm 5.2 \mu\text{M}$), MCF-7 (IC_{50} value of $37.9 \pm 4.9 \mu\text{M}$), and SUM-149 cells (IC_{50} value of $11.8 \pm 4.3 \mu\text{M}$) (Supplementary Fig. S7 online).

SP2043 inhibits MDA-MB-231 tumor growth. Given the inhibition of angiogenesis and lymphangiogenesis by SP2043 (Fig. 1), and the inhibition of breast cancer cell viability (Supplementary Fig. S7 online), we evaluated it for efficacy in animal models of TNBC. MDA-MB-231 tumor xenografts were established in athymic nude mice as previously described^{4,11}. After tumors reached a volume of about 100 mm^3 , SP2043 (10, 20 mg/kg) was administered i.p. every day for up to 33 days. SP2043 significantly inhibits tumor growth: 77.8 and 90.7% inhibition by 10 and 20 mg/kg of SP2043, respectively at day 33 (Fig. 4a). The mouse body weights are statistically identical among those three groups showing no severe toxicity of SP2043 (Supplementary Fig. S4 online). Additional western blot assays show that HGF induces phospho-Met (Y1234/1235) in MDA-MB-231 cells, and SP2043 treatment inhibits this phosphorylation in vitro as in blood and lymphatic endothelial cells (Supplementary Fig. S7 online). To determine if this effect of SP2043 could be detected in vivo, we stained tumor samples from the control and the SP2043 treated groups with anti-phospho-Met (p-Met) antibody and anti-mouse CD31 antibody. Control tumors show ubiquitous p-Met around the mCD31 signal (possibly blood and lymphatic vessels) as well as in cancer cells and other stromal cells (DAPI stained). SP2043 inhibits the amount of p-Met (Supplementary Fig. S7 online). Next, we assessed anti-angiogenic and anti-lymphangiogenic activity of the peptide in the tumors (Fig. 4b–e). Blood vessel (lectin-positive) and lymphatic vessel (LYVE-1 positive) formation is potently inhibited by the peptide (Fig. 4b). Enlarged images from the peri- and intratumoral areas also show the reduction of blood and lymphatic vasculature in the presence of the peptide (Fig. 4c). Pixel based quantification show inhibition of angiogenesis by 57.8% and lymphangiogenesis by 69.5% by SP2043 (Fig. 4d,e).

SP2043 inhibits MDA-MB-231 tumor metastasis in the TCM induced spontaneous metastasis model. We have previously reported that tumor-conditioned media (TCM) pre-treatment followed by tumor inoculation facilitated spontaneous metastasis by influencing lymphangiogenesis and angiogenesis in the primary tumors and pre-metastatic organs^{11,12}. We also previously showed that TCM-induced lymphatic and blood vessel formation in the

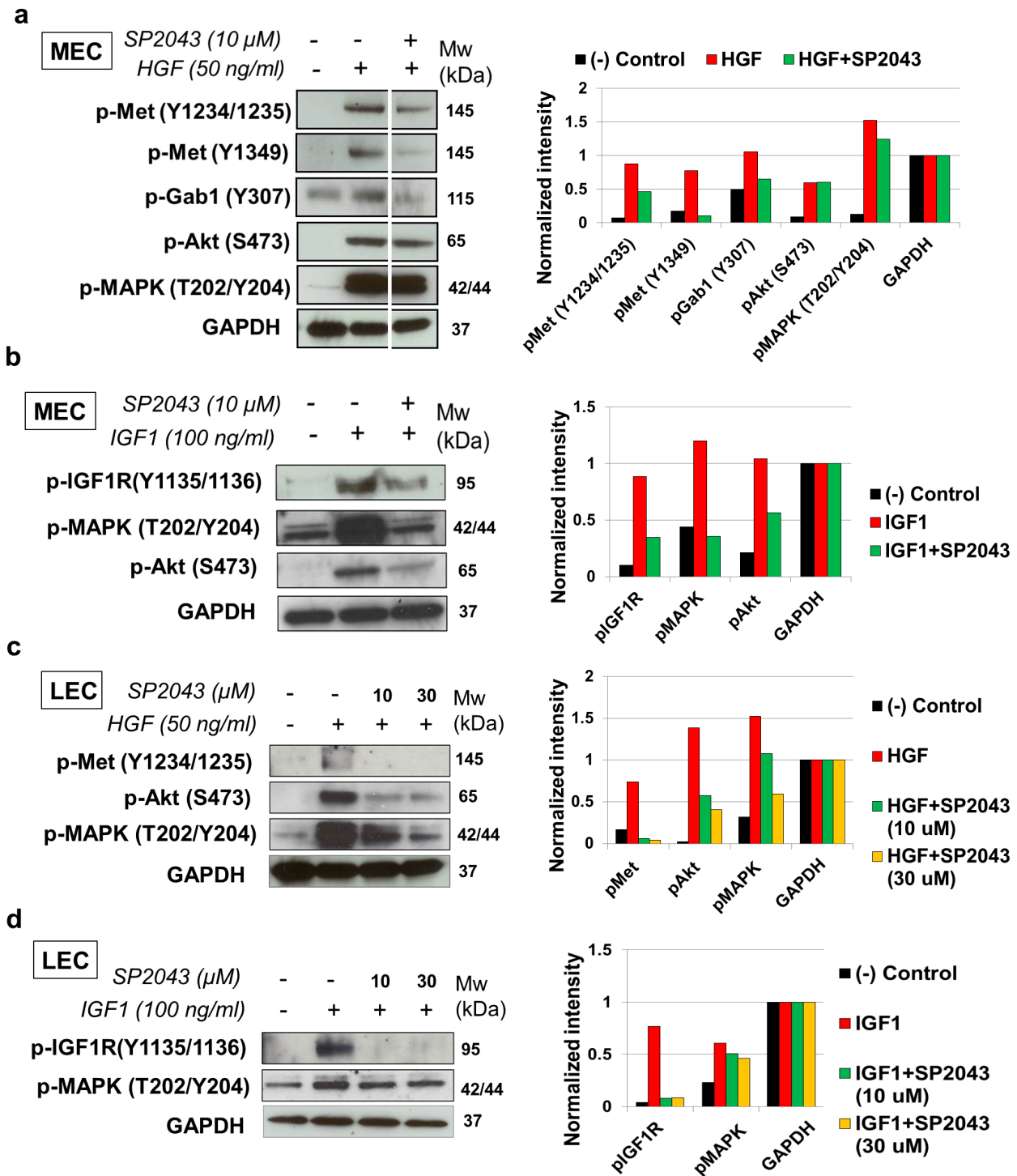


Figure 2 | Inhibition of HGF and IGF1 signals by SP2043. (a) SP2043 blocks HGF-induced phospho-Met (Y1234/1235/1349), phospho-Gab1 (Y307), and phospho-MAPK (T202/204) in MEC. (b) SP2043 blocks IGF1 induced phosphorylation of IGF1R (Y1135/1136), MAPK and Akt (S473) in MEC. (c) SP2043 blocks HGF-induced phosphorylation of Met (Y1234/1235), Akt, and MAPK in LEC. (d) SP2043 also blocks IGF1 induced phosphorylation of IGF1R (Y1135/1136) and MAPK in LEC. All right panels represent GAPDH normalized western intensities. Original gel images of data (a,b,c,d) are presented in Supplementary Fig. S6 online.

brachial lymph nodes was inhibited by treating animals with an anti-lymphangiogenic and anti-angiogenic peptide from the transmembrane 45A (TMEM45A) protein⁴. We hypothesized that SP2043 would show similar inhibitory effects because of its anti-angiogenic and anti-lymphangiogenic properties, preventing the formation of the pre-metastatic niche and subsequent metastasis to these organs. SP2043 was evaluated in the TCM-induced metastasis model (Supplementary Fig. S5 online). Fifty μ l of TCM was subcuta-

neously administered together with or without SP2043 (10 mg/kg, i.p.) for two weeks, after which luciferase-expressing MDA-MB-231 (luc-MDA-MB-231) tumors were established in the inguinal mammary fat pads (Supplementary Fig. S5 online). The primary tumor size is not influenced by either peptide or TCM pre-treatment, as the luc-MDA-MB-231 cancer cells were inoculated after completing the TCM and peptide pre-treatment (Supplementary Fig. S5 online). However, these treatments do significantly

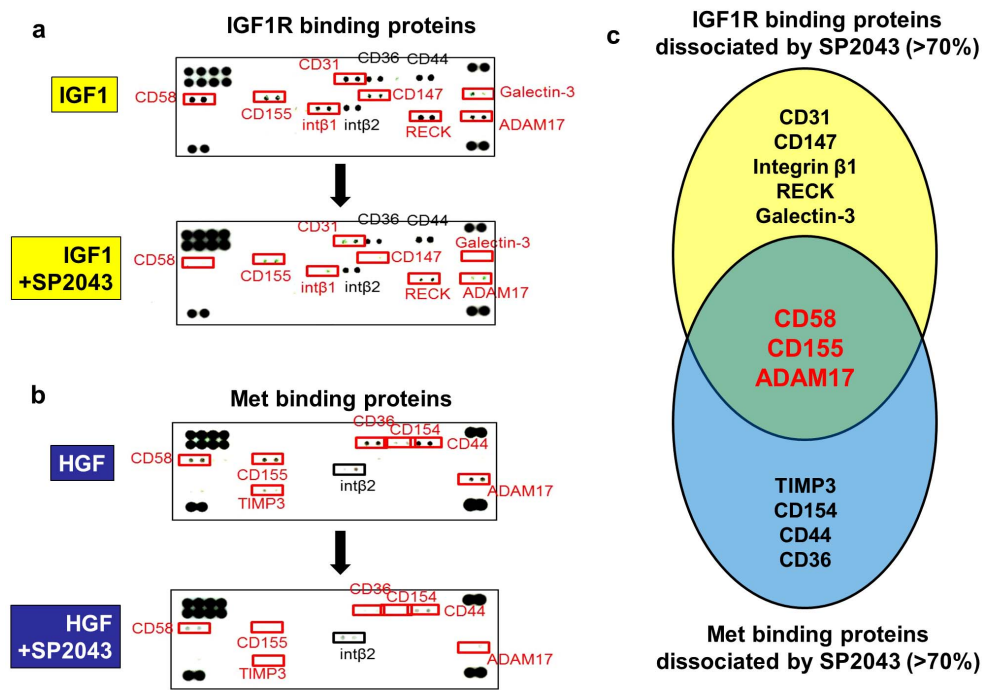


Figure 3 | IGF1R and Met binding receptor proteins. We identified the IGF1R and Met binding receptor proteins that are induced to make a complex by IGF1 and HGF, as well as those that are dissociated by SP2043 treatment. (a) Eleven receptor proteins in the newly formed receptor complex with IGF1R (CD58, CD155, CD31, CD36, CD44, CD147, RECK, ADAM17, Galectin-3, Integrin β 1, Integrin β 2) in response to IGF-1 treatment. After SP2043 treatment, 8 proteins (CD31, CD147, Integrin β 1, RECK, Galectin-3, CD58, CD155, ADAM17) were dissociated from the receptor complex. (b) Eight proteins formed a complex with Met (CD58, CD155, TIMP3, CD36, CD154, CD44, ADAM17, Integrin β 2) in response to HGF treatment. After SP2043 treatment, 7 proteins (CD58, CD155, TIMP3, CD36, CD154, CD44, ADAM17) were dissociated. (c) CD58, CD155, ADAM17 were targeted by SP2043 to dissociate from the receptor complex shown in a Venn diagram.

influence metastatic progression. By week 5, 3 of the 10 mice in the SFM treated group have metastases, in the TCM treated group 9 of the 10 mice have metastases (90%), but in the SP2043 treatment group there are fewer than 50% of metastases compared to the positive control group (Fig. 5a). At week 5, the brachial lymph nodes, lungs, livers, brains, humerus/ulna, and femur/tibia were harvested, bathed in D-luciferin for 5–10 min and imaged using the IVIS imager (Fig. 5b). The LN, lungs, and livers from TCM treated animals show large numbers of metastases while the same tissues from peptide treatment animals have fewer metastases. Since the tumors were inoculated in the inguinal mammary fat pads, only the LN and lung metastasis can be considered to be a result of distant metastasis in the model we used (Supplementary Fig. S5 online). Liver metastasis is a result of adjacent metastasis, as we showed previously in Lee et al¹¹. In that study, inguinal tumor inoculation resulted in abdominal metastasis and the liver and the intestine were the major organs involved in this adjacent metastasis. Luciferase-mediated photon flux from these organs shows that SP2043 significantly blocks lung and LN metastasis (Fig. 5c,d). Antibodies for human vimentin, a marker for metastatic cancer cells²⁶, were used to detect metastases in the LN (Fig. 5e,f). TCM-treated positive LN show macro-metastases (>2 mm), compared to SP2043 treated LN (Fig. 5e). Importantly, the metastases are highly colocalized with the lymphatic endothelium in the LN (Fig. 5f). The enlarged image shows the association of the invading breast cancer cells (red) with the lymphatic vessels (green) in the LN (Fig. 5f), demonstrating that the anti-lymphangiogenic activity of SP2043 inhibited metastasis.

SP2043 inhibits TCM induced lymphangiogenesis and angiogenesis in the lymph nodes and the lungs. To understand the mechanisms of TCM induced metastasis and the inhibition of metastasis by SP2043, we first focused on the lymphangiogenic potency of the MDA-MB-231 TCM in vitro. We tested the effect

of SP2043 on LEC tube formation induced by TCM. TCM promotes LEC tube formation compared to SFM however SP2043 blocks LEC tube formation in a dose response manner (Fig. 6a). We next selected SFM-, TCM-, and SP2043 treated LN and lungs without metastases as confirmed by IVIS imaging. If the organs have metastases, it is difficult to determine whether the angiogenesis and lymphangiogenesis within the organs are induced by systematic injection of TCM or by the local angiogenic and lymphangiogenic factors secreted by the metastases. These selected LN and lungs were analyzed using anti-mouse LYVE-1, and anti-mouse lectin antibodies to detect mouse lymphatic and blood vessels (Fig. 6b). TCM treatment enhances lymphangiogenesis and angiogenesis in the LN as expected. Strikingly, SP2043 treatment inhibits both TCM mediated lymphangiogenesis and angiogenesis in these tissues (Fig. 6b,c). TCM promotes lymphangiogenesis in the lungs, however, blood vessel density is not significantly changed by either TCM or SP2043 treatment (Fig. 6b,d), which can be partially explained by the fact that physiological lungs are already well vascularized²⁷.

Discussion

This study shows that the collagen IV derived biomimetic peptide SP2043 inhibits triple negative breast cancer (TNBC) growth and metastasis. The main mechanism by which SP2043 manifests its anti-cancer effects is by blocking IGF1R and Met signaling in lymphatic and blood endothelial cells. This results in blockage of lymphangiogenesis and angiogenesis in breast cancer primary tumors and in pre-metastatic lungs and lymph nodes, thus inhibiting primary tumor growth and metastasis. Our novel peptide SP2043 (amino acid sequence: LRRFSTAPFAFIDINDVIN) was designed by replacing some natural or synthetic amino acids from our previous collagen IV peptide SP2012 (LRRFSTMPFMF-Abu-NINNV-Abu-NF) for which in vitro and in vivo studies from our laboratory were published

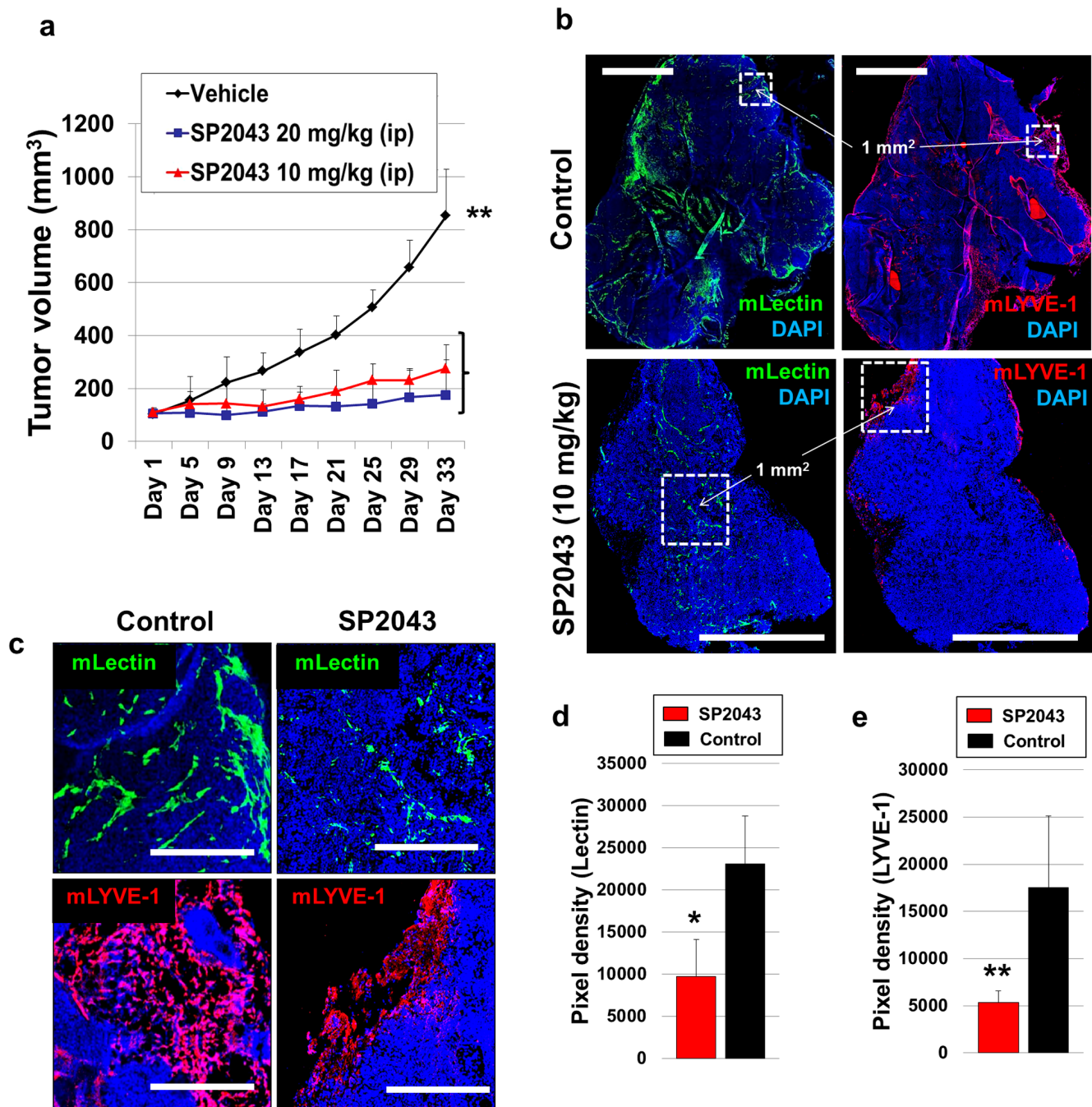


Figure 4 | Inhibition of MDA-MB-231 tumor growth by SP2043. MDA-MB-231 tumor grafted animals were treated with SP2043 (10, 20 mg/kg/day, i.p.) (a) Mean tumor volume. $**P < 0.01$. (b) Tumor tissues were stained with anti-mouse lectin antibodies and anti-mouse LYVE-1 antibodies. Scale bars represent 2,000 μm . White dotted squares are for the enlarged images in (e). (c) Enlarged images. Scale bars represent 500 μm . (d) Quantification of (b) (blood vessels, $*P < 0.05$). (e) Quantification of (b) (lymphatic vessels, $**P < 0.01$). Data (a,d,e) are reported as mean \pm s.e.m.

earlier^{6,8}. These modifications delete the synthetic amino acid Abu (2-aminobutyric acid) and alkyl chain M (methionine), and replace the hydrophobic N (asparagine) with negatively charged D (aspartic acid) for greater water solubility, making the peptide agent translatable and easy to synthesize for the next scale-up step. These modifications were performed based on previous expertise in SAR (Structure & Activity Relationship) analysis in the laboratory^{9,10}.

SP2043 targets both lymphangiogenesis and angiogenesis. Though anti-angiogenic therapies inhibit primary tumor growth, patients suffer from metastasis facilitated by tumor lymphatic vessels which current anti-angiogenic agents, including anti-VEGF agents, are not able to inhibit. In breast cancer, tumor lymphatic vessels are the preferential routes of tumor dissemination²⁸. FDA-approved

anti-lymphangiogenic therapeutic agents have not been developed to date, although a number of anti-angiogenic therapeutic agents are in the clinic and in development. The SP2043 peptide exhibits both anti-lymphangiogenic and anti-angiogenic activity by targeting two different receptor tyrosine kinases: IGF1R and Met in lymphatic and blood endothelial cells (Fig. 2). IGF1R and its contributions to tumor progression have been reported¹⁷. IGF1-PI3K/Akt signaling has been studied in skin cancer progression²⁹. IGF1 regulates the expression of the pituitary tumor transforming gene (PTTG), an oncogene in breast tumor³⁰. Met is also associated with cancer growth, resistance and metastasis. Physiological Met signaling regulates angiogenesis and lymphangiogenesis in ductal carcinoma in situ, thus implicating Met signaling in breast diseases³¹. HGF is a well-known lymphangio-

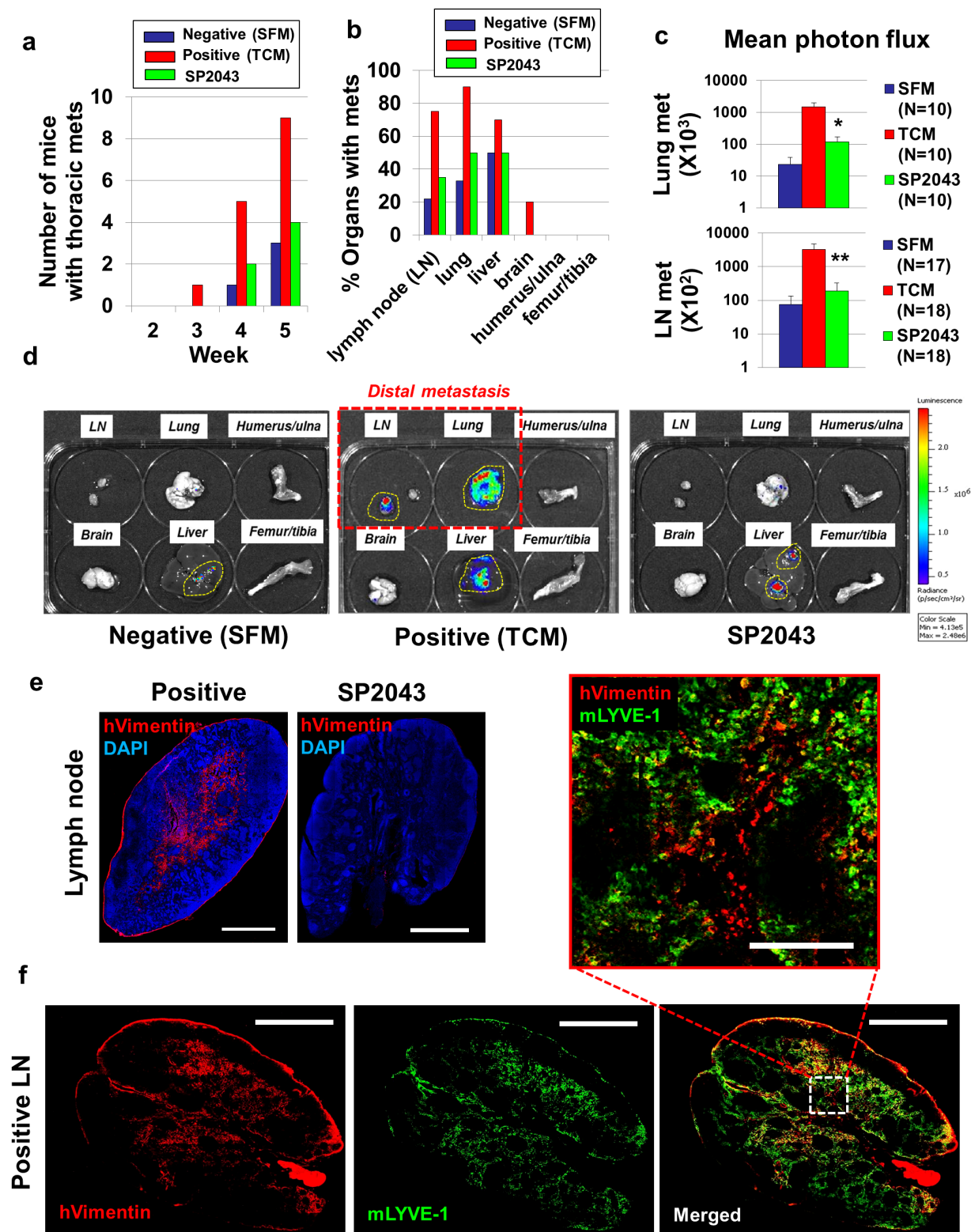


Figure 5 | Inhibition of tumor-conditioned media induced spontaneous metastasis by SP2043. Tumor-conditioned media (TCM) pre-treatment followed by tumor inoculation induce accelerated metastasis formation. SP2043 was administered (10 mg/kg, i.p.) during the TCM induction phase and the resulting effect on metastasis was observed for 5 weeks. (a) Number of mice with thoracic metastasis determined every week. (b) Number of organs with metastases ex vivo at week 5. (c) Mean photon flux from the LN and lungs. Luciferase expressed by MDA-MB-231 cells emit luminescent signal in the presence of D-luciferin (* $P < 0.05$, ** $P < 0.01$). (d) Representative images of the harvested organs. (e) LN metastases. Anti-human vimentin antibodies detect metastatic human breast cancer cells in the LN. LN from animals treated with TCM showed macro-metastases (>2 mm); SP2043 treatment potentially prevents LN metastasis. Scale bars represent 1,000 μ m. (f) Colocalization of the metastases and lymphatic vessels in the LN. Scale bars in the whole images represent 1,000 μ m. Enlarged images also showed this colocalization. The scale bar in the enlarged image represents 200 μ m. Data (c) are reported as mean \pm s.e.m.

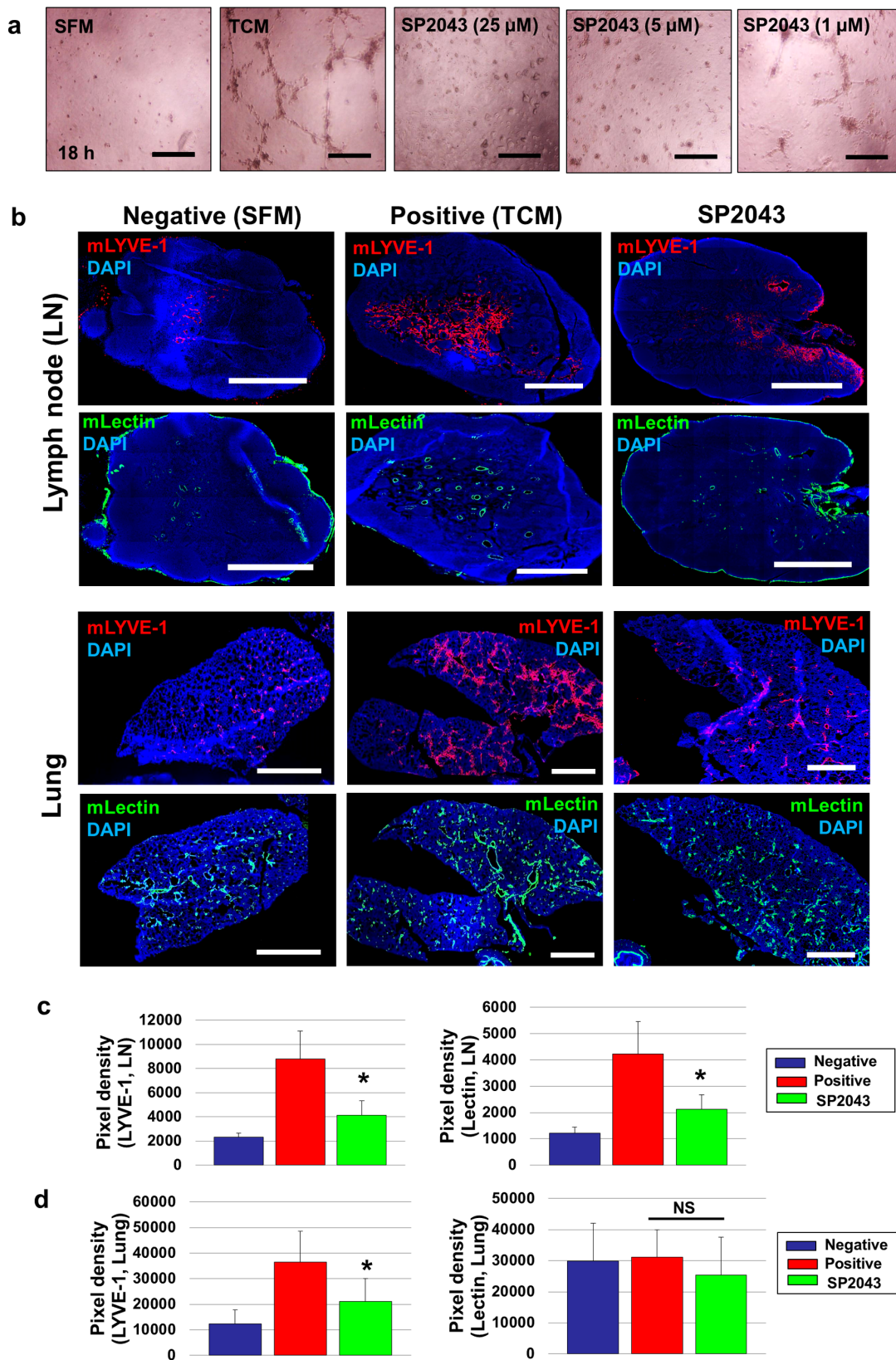


Figure 6 | SP2043 inhibits tumor-conditioned media induced lymphangiogenesis and angiogenesis within pre-metastatic organs. (a) Activity of SP2043 in LEC tube formation induced by TCM at 18 h. SFM was used as a negative control. Scale bars represent 200 μm . (b) From the metastasis models in Fig. 5, we selected SFM-, TCM-, and SP2043-treated LN and lungs without metastases. These selected organs were stained with anti-mouse LYVE-1 and anti-mouse lectin. TCM treated LN showed enhanced lymphangiogenesis and angiogenesis, but SP2043 treatment inhibited them (upper). SP2043 inhibited the increased lymphangiogenesis seen in the lungs of animals treated with TCM. Angiogenesis, however, was not significantly influenced by either TCM or SP2043 (lower). Scale bars represent 1,000 μm . (c) Quantification of (b) upper panels (* $P < 0.05$). (d) Quantification of (b) lower panels (* $P < 0.05$). Data (c,d) are reported as mean \pm s.e.m.



genic factor³², thus the HGF-Met axis has been recognized to have a role in lymphogenous metastasis. For example, intratumoral Met expression is associated with VEGFC expression, lymphangiogenesis, and LN metastasis³³. Recently, Met mediated tumor drug resistance has been reported in several types of cancer^{34–38}. Therefore, the multimodal activity against different receptor tyrosine kinases would be a promising way to overcome tumor-drug resistance that usually arise after using mono-targeted therapies.

We previously reported molecular target data with an earlier version of the peptide, SP2012. In that study, we showed that β 1 integrin is a key target of SP2012 by using a receptor pull-down assay. SP2012 binds to β 1 integrin in cell lysates from HUVEC; however, SP2012 does not bind to cell lysates from HUVEC in which β 1 integrin is knocked down by siRNA⁸. Integrins communicate with multiple receptor-tyrosine kinases (RTKs) and can be targeted for cancer angiogenesis/lymphangiogenesis^{39–41}. This communication is achieved by the formation of a receptor complex that includes integrins and the extracellular parts of particular growth factor receptors as well as other co-receptors. If the peptide binds to domains of integrins resulting in a loosening of the crucial binding pockets or in critical structural changes, the integrins may not appropriately interact with the RTKs and fail to promote signaling from the RTKs. SP2043 differs from SP2012 by 6 amino acids, making SP2043 easier to manufacture and more translational for use in humans. A combination of co-immunoprecipitation and reverse western assays detecting diverse soluble receptors or factors showed that SP2043 treatment disrupts the receptor complexes formed by IGF1R and Met in the presence of IGF1 and HGF (Fig. 3). One interesting point is that the β 1 integrin, which is a target of SP2012^{6,8}, is found to be a co-receptor of only IGF1R upon IGF1 activation, and not in a complex with Met after HGF induction in endothelial cells. Based on these data, we conclude that SP2043 could target more than one receptor in addition to the β 1 integrin, including binding to a new unknown receptor that regulates IGF1R and Met signaling. In the current manuscript, however, we focused on the potent anti-metastatic effects of SP2043 in breast cancer models *in vivo* and identified IGF1R and Met on lymphatic and blood endothelial cells as potential targets. Identification of other possible targets of SP2043 will be the focus of future studies.

The co-receptor data additionally revealed that CD58, CD155, and ADAM17 are completely eliminated after SP2043 treatment from IGF1R and Met co-receptor complexes in the presence of IGF1 and HGF (Fig. 3c). We hypothesize that ADAM17 could be an important target of the SP2043 peptide, as ADAM17 has been widely studied in angiogenesis and cancers^{42,43}, and specifically in breast cancer^{21,44,45}. Although CD58 and CD155 have not been directly implicated in angiogenesis and lymphangiogenesis, CD58 has been reported to promote self-renewal of tumor initiating cells¹⁹, and CD155 is known to induce tumor cell invasion and migration²⁰. Hence CD58 and CD155 could be novel targets of the peptide to directly inhibit breast cancer growth and metastasis. Studies to measure SP2043 peptide binding to/interacting with these receptors and functional assays of angiogenesis, lymphangiogenesis, and tumorigenesis with neutralizing antibodies against these receptors remain subjects for future investigations. This report focuses on the discovery of the dual inhibitory activity of the peptide to efficiently block lymphangiogenesis and angiogenesis, as well as breast cancer growth and metastasis.

SP2043 dramatically inhibits the growth of MDA-MB-231 tumor xenografts (Fig. 4a). The blockade of tumor growth is a result of both the anti-angiogenic (Fig. 4b–d) and possibly anti-tumorigenic activities of SP2043 (Supplementary Fig. S7 online). The peptide also dramatically blocks peri-tumoral lymphangiogenesis in the tumor stroma (Fig. 4e). This is noteworthy for the prevention of metastasis, since the peritumoral lymphatics serve as the initial entry point into the lymphatic system for the dissemination of tumor cells for lymph-

atic metastasis⁴⁶. The SP2043 treatment regimen (10, 20 mg/kg/day, *i.p.* for a month) described in the paper was designed to initially evaluate the therapeutic efficacy of SP2043 in breast tumor models, but this may not be the final formulation of the drug. Most peptide agents may not be sufficiently stable *in vivo*, thus they need to be modified with non-natural amino acids or be encapsulated in appropriate drug carriers to extend their half-life^{47,48}. We have designed PLGA [Poly(D,L-lactide-co-glycolide)] based nanoparticles to load a Serpin derived anti-angiogenic peptide, and the formulation has been tested in mouse models for age-related macular degeneration (AMD)⁴⁹. The encapsulated peptide formulation, which is a more practical solution in the clinic, showed potent therapeutic effects *in vivo*.

As conventional spontaneous metastasis models take more than 2 months to show significant metastasis, tumor-conditioned media (TCM) induced metastasis models were employed (Supplementary Fig. S5 online)^{11,12}. The TCM injection mimics the release of tumor secretions from the primary tumor containing pro-metastatic factors in patients and conditions pre-metastatic organs to prepare them for tumor metastasis. In the orthotopic tumor xenografts established in inguinal mammary fat pads dramatic distal metastasis occurs within 4–5 weeks¹¹. SP2043 (10 mg/kg) was administered *i.p.* only during the 2 week TCM induction phase; it was not administered after tumor inoculation (Supplementary Fig. S5 online). The experiment was designed in this way to determine the efficacy of the peptide in inhibition of metastatic dissemination and colonization by specifically disrupting pre-metastatic niche formation before tumor inoculation. If the peptide was injected after tumor inoculation, the peptide would significantly inhibit tumor growth as well making it difficult to interpret any decrease in metastases. The decrease could have been a result of mechanism based lymphatic and blood vessel targeting or just from the relatively smaller size of the tumors⁵⁰. In this experiment the tumor sizes are identical within all the experimental groups (Supplementary Fig. S5 online). This temporal treatment with SP2043 inhibits only metastatic dissemination and colonization (Fig. 5). LN metastasis is highly correlated with lymphatic vessel density (Fig. 5f) and SP2043 treatment dramatically inhibits lymphangiogenesis and metastasis in the LN of animals treated with TCM (Fig. 6b). Angiogenesis is also crucial for metastatic colonization in the LN as the invading tumor cells require new blood vessels to survive and make colonies at the new location⁵¹. Hence, TCM-induced LN angiogenesis can facilitate tumor metastasis. SP2043 prevents TCM-induced angiogenesis in LN and thus inhibits the growth of the metastases there (Fig. 6c). The lungs are well vascularized organs and so we could not see any dramatic changes in pulmonary angiogenesis after treating with either TCM or SP2043. However, TCM induced lymphatic expansion is significant in the lungs and SP2043 treatment inhibits it (Fig. 6d). Determination of the roles of the lymphatic vessels in the metastatic lungs remains for future studies.

The TCM-induced metastasis model and the anti-metastatic activity of our peptide provide clinical insights and a rationale for using the peptide agent to prevent metastasis in cancer patients in both the adjuvant and neoadjuvant settings. In the neoadjuvant setting, where the tumor is not excised during chemotherapy, the stressed tumor may be secreting factors to promote angiogenesis and lymphangiogenesis at distant sites to allow it to move to a more favorable site where the local tumor microenvironment may protect it. Similarly in the adjuvant setting, although the tumor has been excised, the long-lived factors secreted by the tumor prior to excision could also participate in promoting metastasis by, for example, conditioning the pre-metastatic organs facilitating the circulating tumor cells (CTCs) to invade the organs and colonize them. If the patients are treated with the peptide possibly in combination with chemotherapeutics, CTC proliferation and survival and pre-metastatic niche formation would be inhibited. As a result, secondary recur-



rence of the tumor, including metastases and primary tumor regrowth may be more effectively prevented.

In summary, the anti-lymphangiogenic and anti-angiogenic peptide SP2043 inhibits breast cancer growth and metastasis. As angiogenesis and lymphangiogenesis are central to metastatic cell dissemination and metastatic disease is the primary cause of death in cancer, this peptide could be a potential treatment for metastatic disease.

Methods

Peptide synthesis and handling. SP2043 and scrambled-SP2043 peptides were produced by New England Peptide (Gardner, MA) by using a solid-phase synthesis technique. HPLC and MS analyses of the peptides were provided by the manufacturer to indicate a purity of more than 95%. Peptides were solubilized in 5% DMSO in PBS and the final concentration of DMSO was less than 0.3% in all the experiments. In our previous study, Rosca et al showed that the NINNV sequence in our collagen IV derived biomimetic peptides, e.g., SP2012: LRRFSTMPFMF-Abu-NINNV-Abu-NF, are critical for the activity of the peptide⁵. SP2043 (LRRFSTAPFAFIDINDVINNF) was designed by replacing some natural or synthetic amino acids from SP2012⁵ (LRRFSTMPFMF-Abu-NINNV-Abu-NF) making it easier to manufacture and more translatable. We hypothesized that DINDV in SP2043 is also as critical as NINNV in SP2043 for activity. Therefore, we modified DIND to PEAK to prepare our scrambled-SP2043 (LRRFSTAPFAFPEAKVINNF), and confirmed that this scrambled peptide is much less active than SP2043. (Supplementary Fig. S2 online).

Cell culture. Microvascular endothelial cells (MEC), human umbilical vein endothelial cells (HUVEC), and lymphatic endothelial cells (LEC) were purchased from Lonza (Walkersville, MD) and cultured as described previously⁵. MDA-MB-231, SUM-149, and MCF-7 human breast cancer cell lines were provided by Dr. Zaver Bhujwala (JHMI, Radiology and Oncology). MDA-MB-231-luc-D3H2LN cells were purchased from Caliper (Hopkinton, MA). These breast cancer cells were cultured as described previously^{4,11}.

Cell viability assay. Viability assays using the WST-1 (Roche, Indianapolis, IN) reagent was performed on endothelial cells and breast cancer cells as previously described⁵. Briefly, cancer cells (1,500/well in RPMI-1640) or endothelial cells (2,000/well in EGM) were plated in 96-well plates and incubated overnight. Normal media was replaced with the media with or without peptides and the plates were incubated for 72 h. The controls for cell viability assays correspond to cell phenotypes in normal endothelial growth media (EGM-2 in the HUVEC experiment, or EGM-2MV in LEC and MEC experiments) without peptide treatment. Media was removed and WST-1 solution (1 : 100 diluted in serum-free media) was added. After incubation for 4 h, the absorbance at 450 nm was measured by the Victor V plate reader (Perkin Elmer). IC₅₀ values of the experiments were calculated by using GraphPAD Prism 5 (GraphPad Software Inc.).

Cell migration and adhesion assays. Cell migration and adhesion assays on endothelial cells were performed by using the Real-Time Cell Analysis (RTCA) system (ACEA) as described previously⁵. The ACEA RTCA system measures electrical impedance in real time that is expressed as cell index. When cells are in contact with the gold electrodes, electrical impedance increases. The resulting change in cell index indicates the extent of cell migration from the top compartment to the bottom compartment of a CIM plate, or of cell adhesion to the bottom of the well in an E-plate. In migration, the membrane of the top chamber of a CIM-plate was coated with fibronectin. 180 μL of EGM-2 (HUVEC) or EGM-2MV (LEC or MEC) was added to the bottom chambers, as a chemoattractant. The two chambers were assembled together, 30 μL of serum free media was added to the top chamber and the assembled plate was incubated in a tissue culture incubator at 37°C for 1 h. The equilibrated plate was removed from the incubator and 100 μL of the trypsinized cells (45,000 HUVEC/well; 30,000 MEC/well; 120,000 LEC/well; 200,000) with or without peptides were added to the top chamber. After 30 min incubation at room temperature, the stabilized chamber was loaded in the RTCA machine and the cell index was measured continuously for 20 h. Cell indices at 20 h were selected for analysis. In adhesion assays, 100 μL of 2× concentrated peptide solutions were added to the appropriate wells of an E-plate. LEC or MEC or HUVEC (25,000 cells/well) in 100 μL of EGM-2MV (LEC or MEC) or EGM-2 (HUVEC) media were added next to each well diluting the peptides to the appropriate final concentrations. After equilibrating at room temperature for 30 min, the E-plate was loaded into the RTCA personal system. Cell indices at 3 h were analyzed.

Tube formation assay. Tube formation assays were performed as described previously⁵. 50 μL of Matrigel was loaded in each well of the 96-well plate and the plate was incubated at 37°C for 30 min. Trypsinized HUVEC, LEC, MEC were mixed with the peptide making the appropriate cell density (15,000 cells/well) and peptide concentrations. 100 μL of cell and peptide mixture was added on top of the gel in the 96-well plate. The plate was then incubated at 37°C in a tissue culture incubator and the formation of the capillary-like tubes was observed after 18 h using a Nikon microscope. We quantified tube formation by using Angiogenesis Analyzer for ImageJ (NIH). The process is described in the Supplementary Fig. S8 online. Briefly,

the original jpeg images (three images per group) were transformed to binary images. The binary images were treated with the “fill hole” method to minimize shadow effects. The prepared images were skeletonized. The skeletonized binary tree was analyzed and all the values were normalized with the analyzed area, making the pixel number of the area equal to 100,000 in all the groups. Among several categories of quantification, we chose number of nodes (Nb nodes), Nb junctions, Nb segments, Nb branches. Also we considered length value, including total length (Tot length), Tot branching length, and Tot segment length.

Western blot assay. MEC, LEC and MDA-MB-231 cells were plated on 100 mm tissue culture dishes at 1,000,000 cells/dish. After allowing a day for cell attachment, the cells were starved in serum-free media (SFM) for 24 h, after which SP2043 was added for 90 min. Hepatocyte Growth Factor (HGF) (50 ng/ml) or Insulin-like Growth Factor (IGF1) (100 ng/ml) was added and the incubation was continued for 10–30 min at 37°C. Generation of cell lysates, SDS-PAGE and westerns were done as described in our previous study⁴. The primary antibodies that we used include p-Met (Y1234/1235), p-Met (Y1349), p-Gab1 (Y307), p-Akt (S473), Akt, p-MAPK (T202/Y204), MAPK, p-IGF1R (Y1135/1136), IGF1R, and GAPDH (all from Cell Signaling). All the original images of immunoblot analyses are presented in Supplementary Fig. S6 online.

Identification of IGF1R/Met binding proteins. We hypothesized that the SP2043 peptide binds to unknown receptor proteins on endothelial cells and interrupts both IGF1R and Met. Experiments were designed to determine which receptor proteins make a complex with IGF1R or Met in the presence of IGF1 or HGF and which of these co-receptor proteins are dissociated from IGF1R or Met after treating with SP2043. MEC were plated on tissue culture-treated 100 mm dishes at 1,000,000 cells/dish in EGM-2MV. After allowing a day for cell attachment, the cells were starved in SFM for 24 h, after which SP2043 (30 μM) was added for 90 min. HGF (100 ng/ml) or IGF1 (100 ng/ml) was added and the incubation was continued for 60 min at 37°C. Treatments were stopped by adding cold PBS and cell lysates were prepared using Pierce IP lysis buffer (Thermo Scientific) with 100 μl/ml protease inhibitor (Sigma) and 10 μl/ml phosphatase inhibitors cocktail 2/3 (Sigma). The cell lysates were incubated with the anti-IGF1R or anti-Met antibody (1 : 50, Cell Signaling) overnight, after which protein A/G PLUS agarose (Santa-Cruz) was added and incubated for 3 h to pull down the antibody protein complex. After removing the supernatant and washing with PBS, the PBS-rinsed pellets were treated with glycine (pH 2, 10.0 ml) for 2 h to dissociate all the proteins bound to the beads. The beads were then removed by centrifugation. To allow the proteins to recover their structures and to maintain normal pH, 0.5 ml of Tris (pH 8) was added. The mixture was dialyzed with Amicon Ultra 3K filter units (Millipore) to remove glycine and Tris. The resulting mixture was analyzed using reverse antibody arrays for human soluble receptors (Proteome Profiler Antibody Arrays Kit for human soluble receptors, R&D systems) following the product manual.

MDA-MB-231 tumor xenografts. MDA-MB-231 tumor xenografts were established as described previously⁴. SP2043 (10 or 20 mg/kg) or vehicle was injected daily intraperitoneally (i.p.), and the administration was continued for 33 days. The tumor size and mouse body weight were measured every four days. The tumor volume was calculated by using the formula: $V = 0.52 \times (\text{'long axis' of the tumor}) \times (\text{'short axis' of the tumor})^2$.

TCM-induced spontaneous metastasis models. The tumor-conditioned media (TCM) induced spontaneous metastasis model that we previously developed¹¹ was used to accomplish accelerated metastasis and to evaluate the anti-metastatic effects of SP2043. MDA-MB-231-luc-D3H2LN tumor-conditioned media (TCM) was prepared as previously described¹¹. Fifty μl TCM or SFM was administered daily subcutaneously through the scruff of 4–5 week old female athymic nude mice for two weeks. TCM treated animals were either treated with SP2043 (10 mg/kg, i.p.) or with the vehicle during the TCM induction phase. Then, 2×10^6 MDA-MB-231-luc-D3H2LN cells in 100 μl of 50% matrigel were orthotopically inoculated into the upper inguinal mammary fat pad of these TCM conditioned mice under anesthesia (50 mg/kg ketamine + 5 mg/kg acepromazine in PBS, i.p. injection). After two weeks, the primary tumor size was measured, and thoracic metastasis was assessed every week by using the In Vivo Imaging System (IVIS) Xenogen 200 optical imager (Xenogen) as described previously¹¹. After 5 weeks, the lungs, brains, livers, brachial lymph nodes, humerus/ulna, and femur/tibia were harvested and bathed in D-luciferin solution for 3 min and placed in the IVIS imager to detect metastases ex vivo. Luciferase-mediated photon flux ex vivo was quantified by using Living Image® 3D Analysis (Xenogen).

Immunofluorescence. Immunofluorescence was performed following the protocol described previously¹¹. Primary antibodies that we used include: rabbit anti-mouse LYVE-1 antibody (1 : 200, AngioBio), rat anti-mouse CD31 (1 : 100, BD Pharmingen), rabbit anti-phospho-Met (1 : 400, Cell Signaling), mouse anti-human PCNA (1 : 100, BD Pharmingen), mouse anti-human vimentin (1 : 50, Santa Cruz), and goat anti-mouse lectin FITC (1 : 100, Sigma). Secondary antibodies include: FITC-conjugated goat anti-rat, FITC-conjugated goat anti-rabbit, rhodamine-conjugated goat anti-mouse, Cy3-conjugated goat anti-rabbit, and Alexa Fluor 488 goat anti-rabbit (1 : 500, all from Jackson ImmunoResearch). Fluorescent signals were visualized and digital images were obtained using the LSM-510 confocal microscope (Carl Zeiss). We quantified the images using ImageJ (NIH, Bethesda, MD), measuring



the pixel number/10× frame of randomly selected 12 images in each sample. Each group included at least three different samples.

Statistical analysis. Error bars correspond to SEM, unless otherwise stated. Differences between the control and the peptide treated group are regarded as significant when P is less than 0.05 using the Student's t-test.

- DeSantis, C., Ma, J., Bryan, L. & Jemal, A. Breast cancer statistics, 2013. *CA Cancer J Clin* **64**, 52–62 (2014).
- Shamloo, B. K. *et al.* Novel adverse events of bevacizumab in the US FDA adverse event reporting system database: a disproportionality analysis. *Drug Saf* **35**, 507–518 (2012).
- Schoppmann, S. F. *et al.* Prognostic value of lymphangiogenesis and lymphovascular invasion in invasive breast cancer. *Ann Surg* **240**, 306–312 (2004).
- Lee, E., Koskimaki, J. E., Pandey, N. B. & Popel, A. S. Inhibition of lymphangiogenesis and angiogenesis in breast tumor xenografts and lymph nodes by a peptide derived from transmembrane protein 45A. *Neoplasia* **15**, 112–124 (2013).
- Lee, E., Rosca, E. V., Pandey, N. B. & Popel, A. S. Small peptides derived from somatotropin domain-containing proteins inhibit blood and lymphatic endothelial cell proliferation, migration, adhesion and tube formation. *Int J Biochem Cell Biol* **43**, 1812–1821 (2011).
- Koskimaki, J. E. *et al.* Synergy between a collagen IV mimetic peptide and a somatotropin-domain derived peptide as angiogenesis and lymphangiogenesis inhibitors. *Angiogenesis* **16**, 159–170 (2013).
- Karagiannis, E. D. & Popel, A. S. A systematic methodology for proteome-wide identification of peptides inhibiting the proliferation and migration of endothelial cells. *Proc Natl Acad Sci U S A* **105**, 13775–13780 (2008).
- Rosca, E. V., Koskimaki, J. E., Pandey, N. B., Wolff, A. C. & Popel, A. S. Development of a biomimetic peptide derived from collagen IV with anti-angiogenic activity in breast cancer. *Cancer Biol Ther* **12**, 808–817 (2011).
- Rosca, E. V., Koskimaki, J. E., Pandey, N. B., Tamiz, A. P. & Popel, A. S. Structure-activity relationship study of collagen-derived anti-angiogenic biomimetic peptides. *Chem Biol Drug Des* **80**, 27–37 (2012).
- Rivera, C. G. *et al.* Novel peptide-specific quantitative structure-activity relationship (QSAR) analysis applied to collagen IV peptides with antiangiogenic activity. *J Med Chem* **54**, 6492–6500 (2011).
- Lee, E., Pandey, N. B. & Popel, A. S. Pre-treatment of mice with tumor-conditioned media accelerates metastasis to lymph nodes and lungs: a new spontaneous breast cancer metastasis model. *Clin Exp Metastasis* **31**, 67–79 (2014).
- Lee, E. *et al.* Breast cancer cells condition lymphatic endothelial cells within pre-metastatic niches to promote metastasis. *Nat Commun* **5**, 4715 (2014).
- Oommen, S., Gupta, S. K. & Vlahakis, N. E. Vascular endothelial growth factor A (VEGF-A) induces endothelial and cancer cell migration through direct binding to integrin $\alpha_9\beta_1$: identification of a specific $\alpha_9\beta_1$ binding site. *J Biol Chem* **286**, 1083–1092 (2011).
- Mitra, A. K. *et al.* Ligand-independent activation of c-Met by fibronectin and $\alpha_5\beta_1$ -integrin regulates ovarian cancer invasion and metastasis. *Oncogene* **30**, 1566–1576 (2011).
- Kabir-Salmami, M., Shiokawa, S., Akimoto, Y., Sakai, K. & Iwashita, M. The role of $\alpha_5\beta_1$ -integrin in the IGF-I-induced migration of extravillous trophoblast cells during the process of implantation. *Mol Hum Reprod* **10**, 91–97 (2004).
- Yu, X., Miyamoto, S. & Mekada, E. Integrin $\alpha_2\beta_1$ -dependent EGF receptor activation at cell-cell contact sites. *J Cell Sci* **113** (Pt 12), 2139–2147 (2000).
- Bahr, C. & Groner, B. The IGF-1 receptor and its contributions to metastatic tumor growth—novel approaches to the inhibition of IGF-1R function. *Growth Factors* **23**, 1–14 (2005).
- Sennino, B., Ishiguro-Oonuma, T., Schriver, B. J., Christensen, J. G. & McDonald, D. M. Inhibition of c-Met reduces lymphatic metastasis in RIP-Tag2 transgenic mice. *Cancer Res* **73**, 3692–3703 (2013).
- Xu, S. *et al.* CD58, a novel surface marker, promotes self-renewal of tumor-initiating cells in colorectal cancer. *Oncogene* (2014) doi: 10.1038/onc.2014.95. [Epub ahead of print].
- Sloan, K. E. *et al.* CD155/PVR plays a key role in cell motility during tumor cell invasion and migration. *BMC Cancer* **4**, 73 (2004).
- Glunde, K. & Stasinopoulos, I. ADAM17: the new face of breast cancer-promoting metalloprotease activity. *Cancer Biol Ther* **8**, 1055–1057 (2009).
- Pacher, M. *et al.* Impact of constitutive IGF1/IGF2 stimulation on the transcriptional program of human breast cancer cells. *Carcinogenesis* **28**, 49–59 (2007).
- Peyrat, J. P. *et al.* Characterization of insulin-like growth factor 1 receptors (IGF1-R) in human breast cancer cell lines. *Bull Cancer* **76**, 311–319 (1989).
- Parr, C. & Jiang, W. G. Hepatocyte growth factor activation inhibitors (HAI-1 and HAI-2) regulate HGF-induced invasion of human breast cancer cells. *Int J Cancer* **119**, 1176–1183 (2006).
- Sakai, K., Yamashita, J. & Ogawa, M. [A strong predictor of breast cancer--hepatocyte growth factor (HGF)]. *Gan To Kagaku Ryoho* **22 Suppl 1**, 71–74 (1995).
- Vora, H. H. *et al.* Cytokeratin and vimentin expression in breast cancer. *Int J Biol Markers* **24**, 38–46 (2009).
- Hoganson, D. M., Pryor, H. L., 2nd & Vacanti, J. P. Tissue engineering and organ structure: a vascularized approach to liver and lung. *Pediatr Res* **63**, 520–526 (2008).
- Cao, Y. Opinion: emerging mechanisms of tumour lymphangiogenesis and lymphatic metastasis. *Nat Rev Cancer* **5**, 735–743 (2005).
- Wilker, E. *et al.* Role of PI3K/Akt signaling in insulin-like growth factor-1 (IGF-1) skin tumor promotion. *Mol Carcinog* **44**, 137–145 (2005).
- Thompson, A. D., 3rd & Kakar, S. S. Insulin and IGF-1 regulate the expression of the pituitary tumor transforming gene (PTTG) in breast tumor cells. *FEBS Lett* **579**, 3195–3200 (2005).
- Gotte, M., Kersting, C., Radke, I., Kiesel, L. & Wulfig, P. An expression signature of syndecan-1 (CD138), E-cadherin and c-met is associated with factors of angiogenesis and lymphangiogenesis in ductal breast carcinoma in situ. *Breast Cancer Res* **9**, R8 (2007).
- Saito, Y. *et al.* Transfection of human hepatocyte growth factor gene ameliorates secondary lymphedema via promotion of lymphangiogenesis. *Circulation* **114**, 1177–1184 (2006).
- Zhao, D. *et al.* Intratumoral c-Met expression is associated with vascular endothelial growth factor C expression, lymphangiogenesis, and lymph node metastasis in oral squamous cell carcinoma: implications for use as a prognostic marker. *Hum Pathol* **42**, 1514–1523 (2011).
- Maroun, C. R. & Rowlands, T. The Met receptor tyrosine kinase: a key player in oncogenesis and drug resistance. *Pharmacol Ther* **142**, 316–338 (2014).
- Krumbach, R. *et al.* Primary resistance to cetuximab in a panel of patient-derived tumour xenograft models: activation of MET as one mechanism for drug resistance. *Eur J Cancer* **47**, 1231–1243 (2011).
- Etnyre, D. *et al.* Targeting c-Met in melanoma: Mechanism of resistance and efficacy of novel combinatorial inhibitor therapy. *Cancer Biol Ther* **15**, 1129–1141 (2014).
- Paulson, A. K. *et al.* MET and ERBB2 are coexpressed in ERBB2+ breast cancer and contribute to innate resistance. *Mol Cancer Res* **11**, 1112–1121 (2013).
- Mueller, K. L. *et al.* Fibroblast-secreted hepatocyte growth factor mediates epidermal growth factor receptor tyrosine kinase inhibitor resistance in triple-negative breast cancers through paracrine activation of Met. *Breast Cancer Res* **14**, R104 (2012).
- Desgrosellier, J. S. & Cheresch, D. A. Integrins in cancer: biological implications and therapeutic opportunities. *Nat Rev Cancer* **10**, 9–22 (2010).
- Avraamides, C. J., Garmy-Susini, B. & Varner, J. A. Integrins in angiogenesis and lymphangiogenesis. *Nat Rev Cancer* **8**, 604–617 (2008).
- Soung, Y. H., Clifford, J. L. & Chung, J. Crosstalk between integrin and receptor tyrosine kinase signaling in breast carcinoma progression. *BMB Rep* **43**, 311–318 (2010).
- Lin, J. *et al.* ADAM17 overexpression promotes angiogenesis by increasing blood vessel sprouting and pericyte number during brain microvessel development. *Int J Dev Biol* **55**, 961–968 (2011).
- Das, S. *et al.* ADAM17 silencing in mouse colon carcinoma cells: the effect on tumoricidal cytokines and angiogenesis. *PLoS One* **7**, e50791 (2012).
- Zheng, X. *et al.* ADAM17 promotes breast cancer cell malignant phenotype through EGFR-PI3K-AKT activation. *Cancer Biol Ther* **8**, 1045–1054 (2009).
- Gao, M. Q. *et al.* Human breast cancer-associated fibroblasts enhance cancer cell proliferation through increased TGF- α cleavage by ADAM17. *Cancer Lett* **336**, 240–246 (2013).
- Padera, T. P. *et al.* Lymphatic metastasis in the absence of functional intratumor lymphatics. *Science* **296**, 1883–1886 (2002).
- Rosca, E. V. *et al.* Anti-angiogenic peptides for cancer therapeutics. *Curr Pharm Biotechnol* **12**, 1101–1116 (2011).
- Bhise, N. S., Shmueli, R. B., Sunshine, J. C., Tzeng, S. Y. & Green, J. J. Drug delivery strategies for therapeutic angiogenesis and antiangiogenesis. *Expert Opin Drug Deliv* **8**, 485–504 (2011).
- Shmueli, R. B. *et al.* Long-term suppression of ocular neovascularization by intraocular injection of biodegradable polymeric particles containing a serpin-derived peptide. *Biomaterials* **34**, 7544–7551 (2013).
- Ito, Y. *et al.* Tumor size is the strongest predictor of microscopic lymph node metastasis and lymph node recurrence of N0 papillary thyroid carcinoma. *Endocr J* **60**, 113–117 (2013).
- Hood, J. L., San, R. S. & Wickline, S. A. Exosomes released by melanoma cells prepare sentinel lymph nodes for tumor metastasis. *Cancer Res* **71**, 3792–3801 (2011).

Acknowledgments

We thank Dr. Zaver Bhujwala for providing MDA-MB-231, SUM-149, and MCF-7 breast cancer cell lines for this study and Dr. Yama Abasi and ACEA Biosciences for the use of the RTCA system for measuring cell migration and adhesion. This work was supported by the National Institutes of Health grants R01 CA138264, R21 CA152473, and the Safeway Foundation.



Author contributions

E.L., N.B.P. and A.S.P. conceived the work. E.L. performed most of the experiments. S.J.L. performed western blot assays with blood and lymphatic endothelial cells. J.E.K. performed HUVEC viability, migration and adhesion assays. Z.H. performed western blot assays with breast cancer cells. E.L., S.J.L., J.E.K., Z.H., N.B.P. and A.S.P. interpreted the experimental data. E.L. wrote the manuscript, and E.L., N.B.P. and A.S.P. edited the manuscript.

Additional information

Supplementary information accompanies this paper at <http://www.nature.com/scientificreports>

Competing financial interests: Yes there is potential Competing Interest. ASP is a co-founder and serves as the CSO of AsclepiX Therapeutics, LLC; the terms of this

arrangement are being managed by the Johns Hopkins University in accordance with its conflict of interest policies.

How to cite this article: Lee, E. *et al.* Inhibition of breast cancer growth and metastasis by a biomimetic peptide. *Sci. Rep.* **4**, 7139; DOI:10.1038/srep07139 (2014).



This work is licensed under a Creative Commons Attribution-NonCommercial-ShareAlike 4.0 International License. The images or other third party material in this article are included in the article's Creative Commons license, unless indicated otherwise in the credit line; if the material is not included under the Creative Commons license, users will need to obtain permission from the license holder in order to reproduce the material. To view a copy of this license, visit <http://creativecommons.org/licenses/by-nc-sa/4.0/>

Supplementary Information

Inhibition of breast cancer growth and metastasis by a biomimetic peptide

Esak Lee^a, Seung Jae Lee^a, Jacob E. Koskimaki^a, Zheyi Han^a, Niranjan B. Pandey^a, and Aleksander S. Popel^{a,b}

^aDepartment of Biomedical Engineering, Johns Hopkins University School of Medicine, Baltimore, MD 21205, United States.

^bDepartment of Oncology and the Sidney Kimmel Comprehensive Cancer Center, Johns Hopkins University School of Medicine, Baltimore, MD 21231, United States.

Contents

Supplementary Figures

Figure S1: In vitro activity of SP2043 on MEC and LEC	3
Figure S2: Scrambled SP2043 is inactive, compared to SP2043	4
Figure S3: SP2043 does not inhibit EGFR signaling.	5
Figure S4: Body weight of SP2043 treated animals over the course of the study	6
Figure S5: Tumor-conditioned media induced spontaneous metastasis model	7
Figure S6: Original gel images of immunoblot analysis.	8
Figure S7: Peptide activity in breast tumor cells	10
Figure S8: Tube formation analysis	11

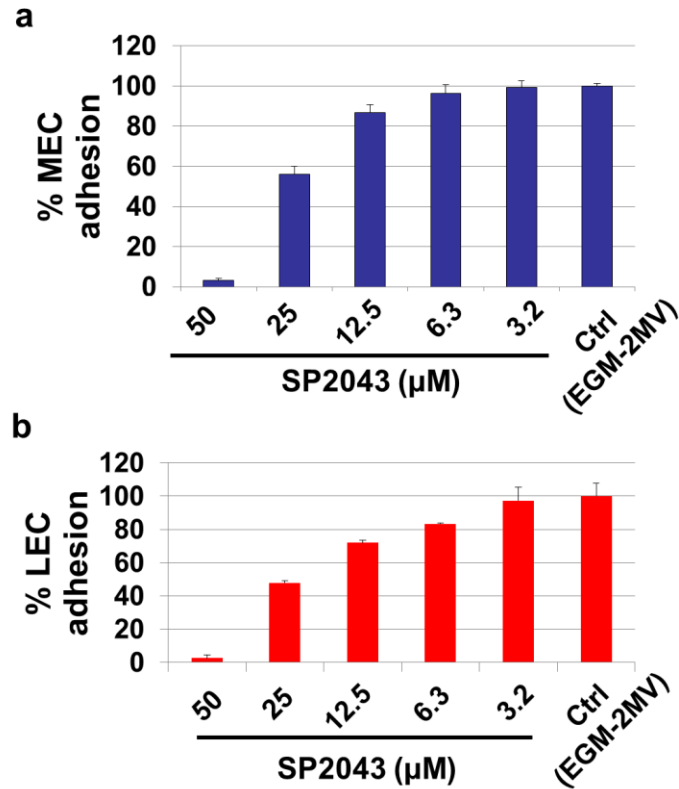


Figure S1: In vitro activity of SP2043 on MEC and LEC. MEC and LEC adhesion was assessed in the presence of the SP2043 peptide, using the ACEA E-plate and real time cell analysis (RTCA) system. 100 μl of 2X concentrated peptide solution was added to the appropriate wells of an E-plate (ACEA). LEC and MEC (25,000 cells/well) in EGM-2MV (LEC, MEC) were then added to each well diluting the peptides to the appropriate final concentration. After equilibrating at room temperature for 30 min, the E-plate was loaded into the RTCA system. Cell indices at 3 h were analyzed. SP2043 inhibits MEC and LEC adhesion. **(a)** Percent MEC adhesion. **(b)** Percent LEC adhesion.

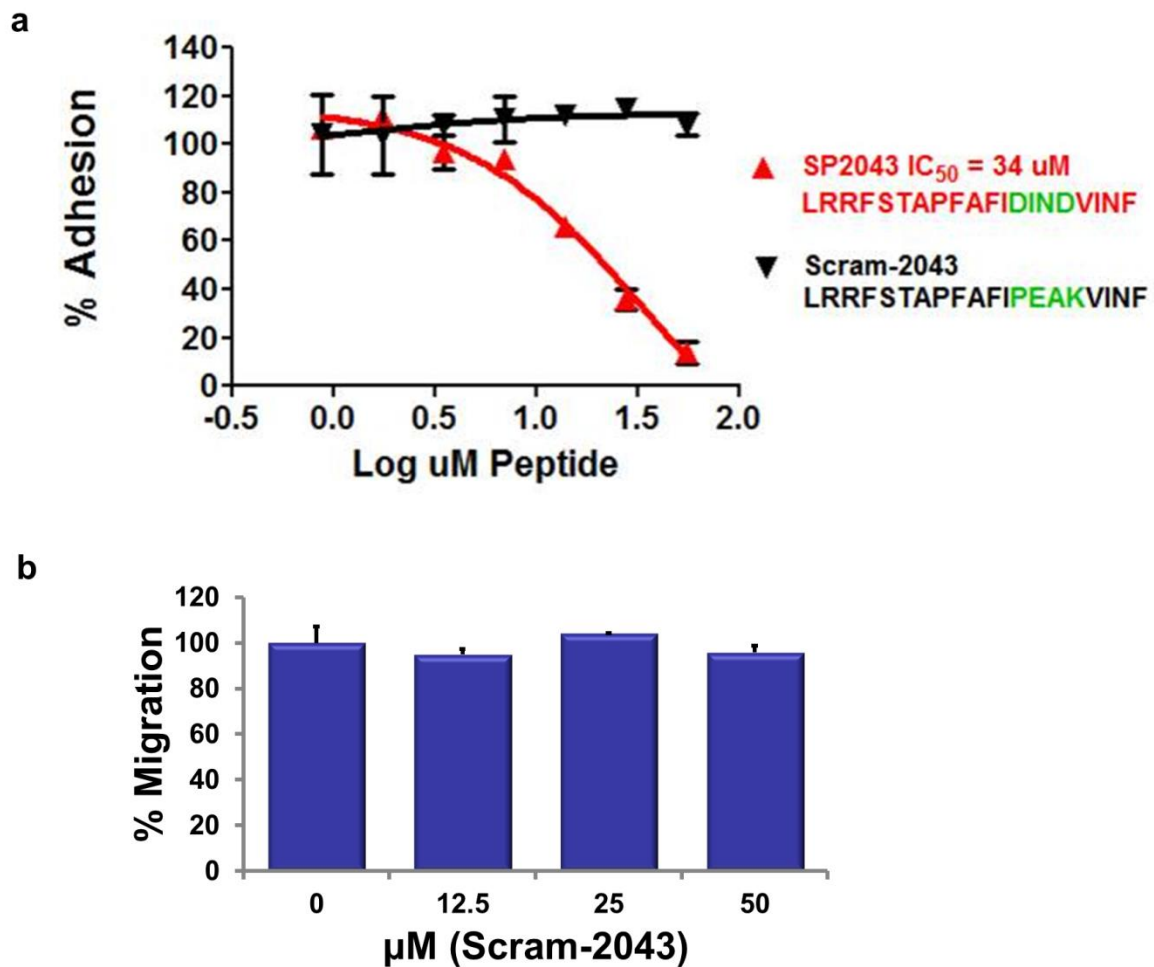


Figure S2: Scrambled SP2043 is inactive, compared to SP2043. Inactive peptide was prepared and tested in MEC adhesion and migration. **(a)** MEC adhesion. SP2043 inhibits MEC adhesion in dose responsive manners, but scrambled-SP2043 (Scram-2043) is inactive, demonstrating the SP2043 peptide activity is not derived from non-specific and sticky properties of peptides. **(b)** MEC migration with the Scram-2043.

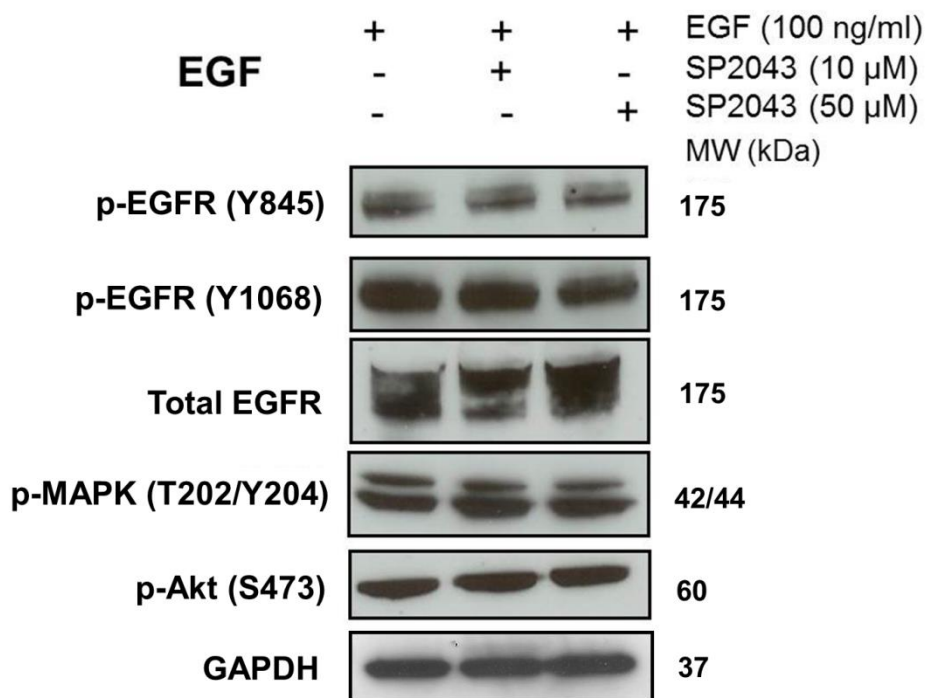


Figure S3: SP2043 does not inhibit EGFR signaling. MDA-MB-231 cells were treated with EGF in the presence of SP2043 and EGF. p-EGFR (Y845, Y1608), p-MAPK (T202/Y204) and p-Akt (S473) were assessed, and we observed that SP2043 does not block EGF-EGFR signaling pathways. Original gel images of data are presented in Supplementary Fig. S6.

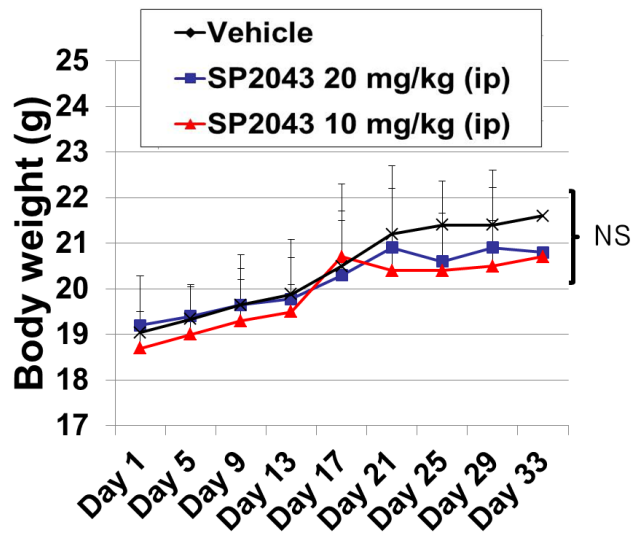


Figure S4: Body weight of SP2043 treated animals over the course of the study.

Two million MDA-MB-231 cells were orthotopically inoculated into athymic nude mice, and the tumors were allowed to grow until they reached a size of approximately 100 mm³. SP2043 (10 or 20 mg/kg) or vehicle were injected intraperitoneally (i.p.), and the body weights of the animals were measured every four days using a weighing machine for small animals. The body weights of the SP2043 treated animals were similar to that of the control animals, showing that the peptide treatment is not toxic.

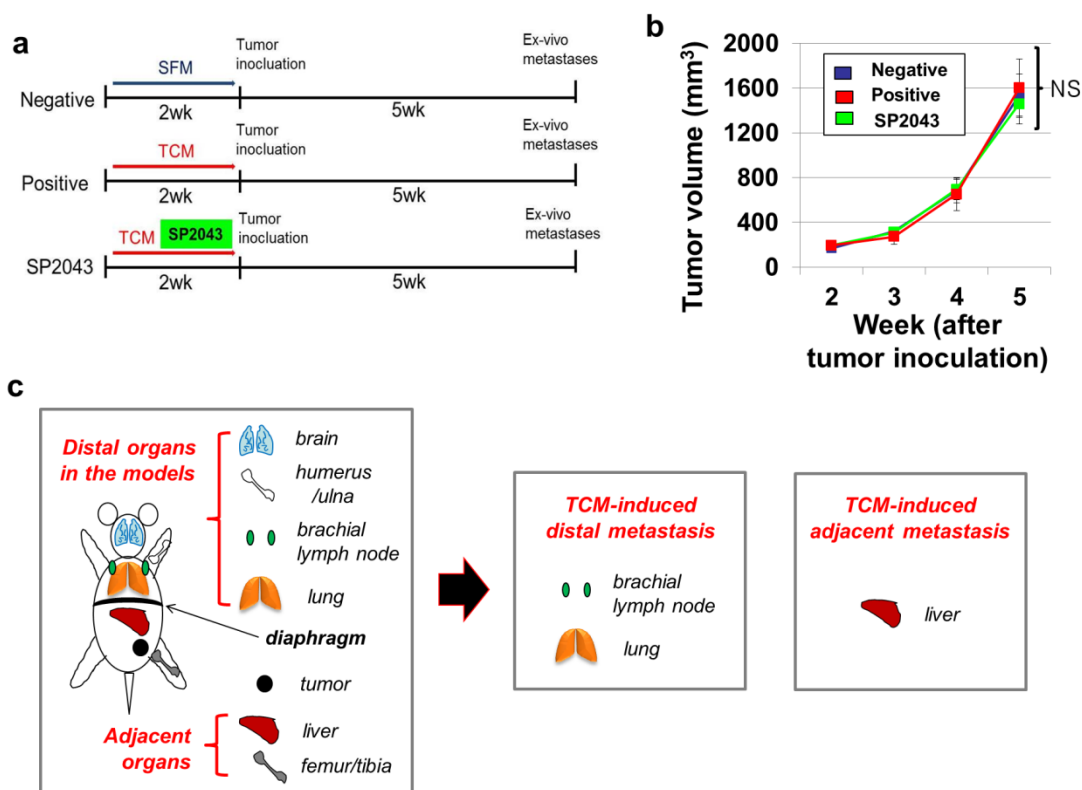


Figure S5: Tumor-conditioned media induced spontaneous metastasis model.

Tumor-conditioned media (TCM) pre-treatment followed by tumor inoculation induce metastasis formation within a month. SP2043 was administered (10 mg/kg, i.p.) in the TCM induction phase. **(A)** Experimental group description. **(B)** Mean tumor volumes. **(C)** Description of organ metastasis. Inguinal tumors were established in mice. Only the brachial lymph node and lung metastasis are considered to constitute distant metastasis, since they are sufficiently far from the inguinal primary tumors. Liver metastases are involved with abdominal metastasis and can be regarded as adjacent metastasis.

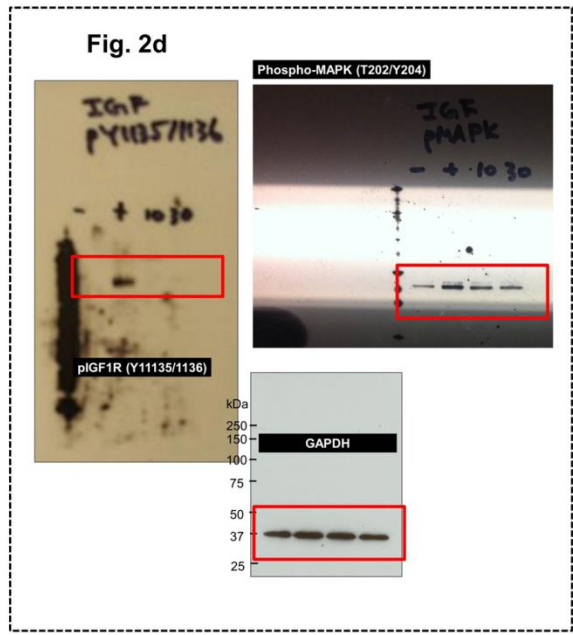
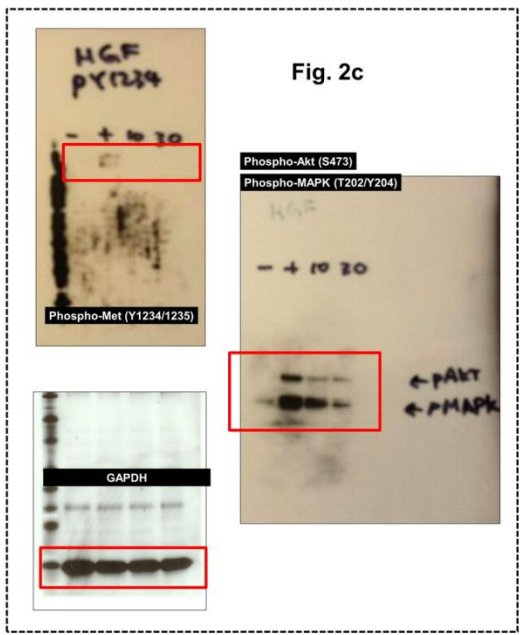
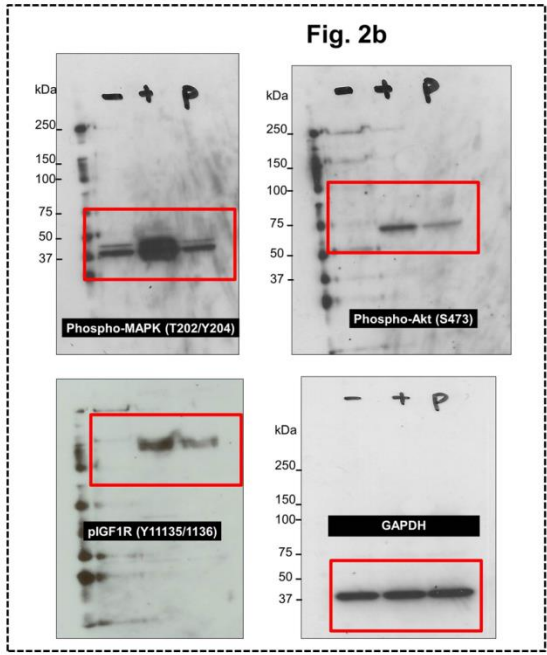
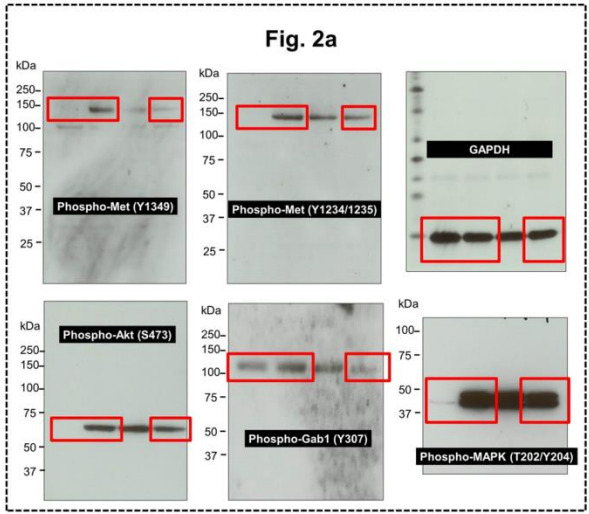


Figure S6: Original gel images of immunoblot analysis.

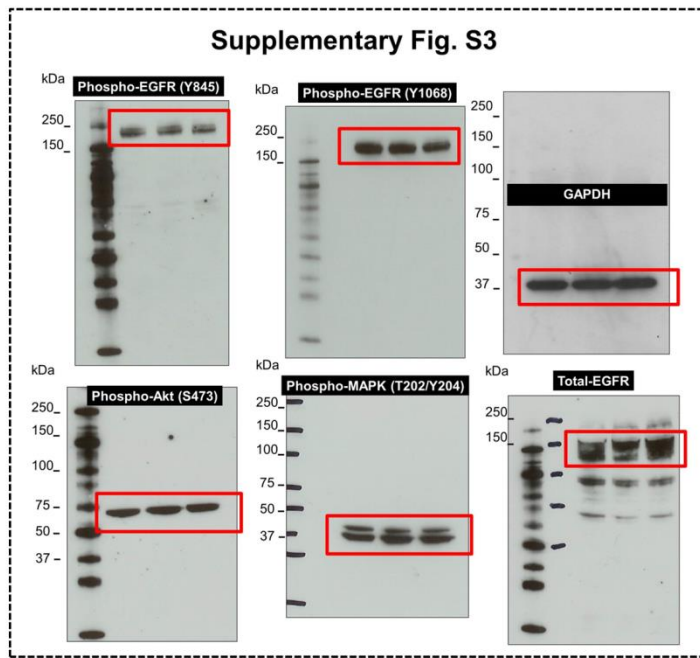
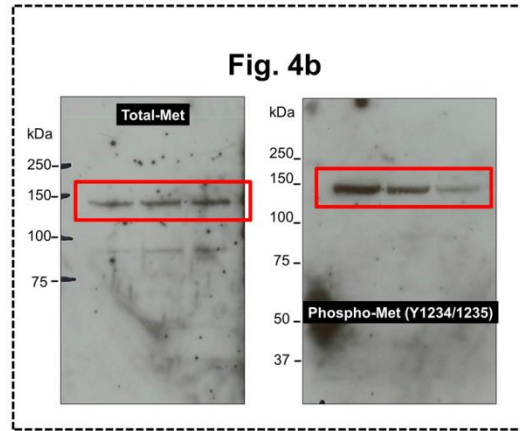


Figure S6: Original gel images of immunoblot analysis (continued).

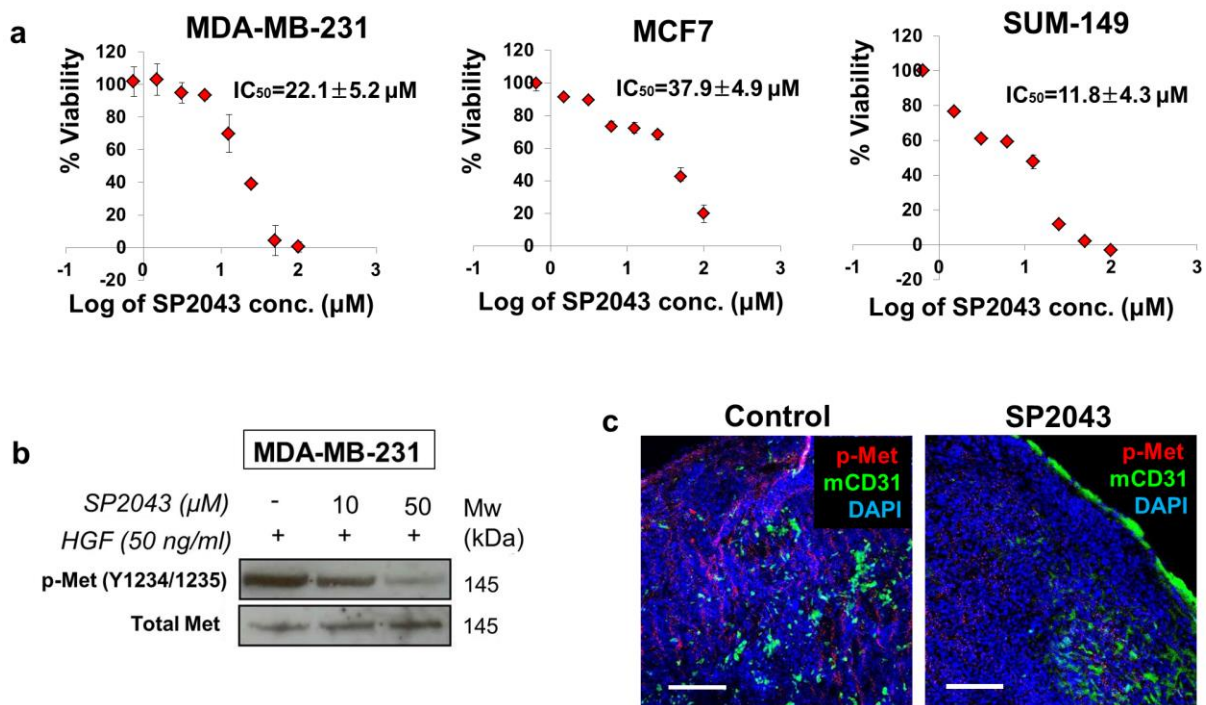
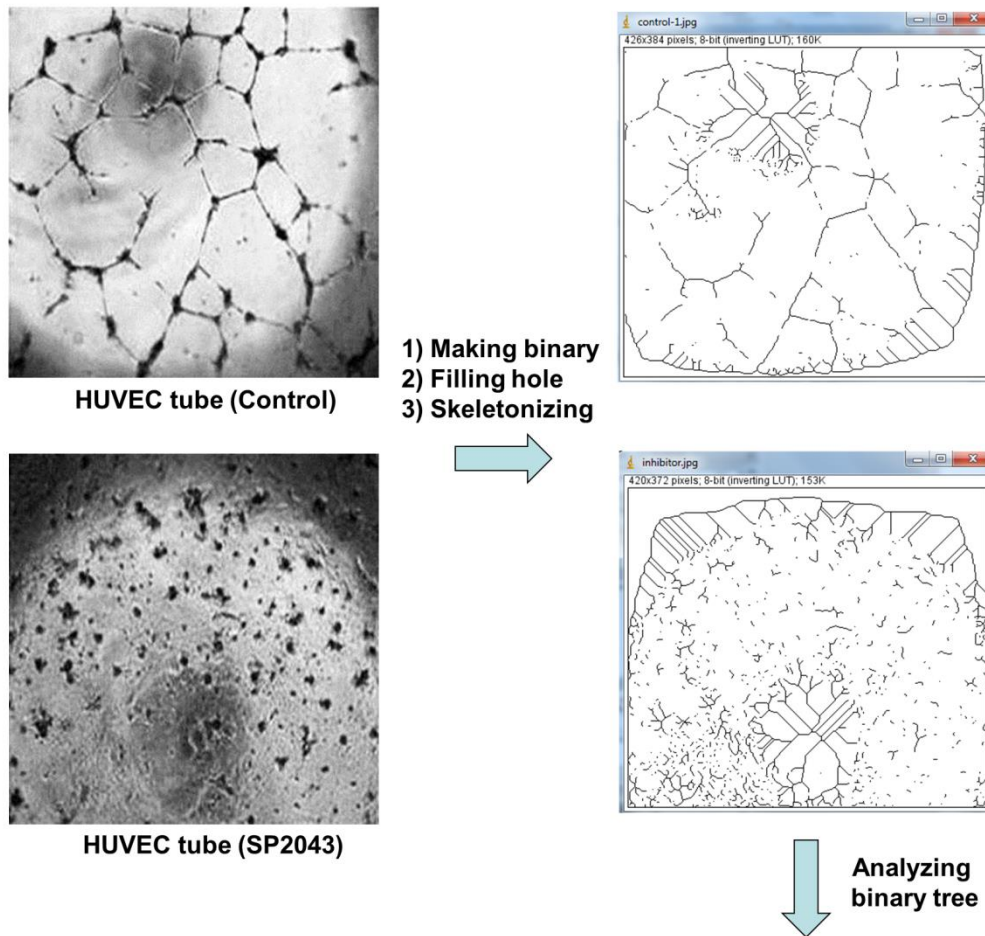


Figure S7: Peptide activity in breast tumor cells

(a) Inhibition of breast cancer cell viability by SP2043. The peptide inhibited viability of MDA-MB-231, MCF-7, and SUM-149 cells. (b) In vitro western blot assays with MDA-MB-231 cells. HGF (50 ng/ml) treated MDA-MB-231 cells showed an increase in the amount of phospho-Met which was inhibited by peptide treatment. (c) Inhibition of phosphorylation of Met in vivo observed by immunostaining tumor tissues with anti-phospho-Met antibodies and mCD31 antibodies. Control tumors have ubiquitous p-Met, compared to SP2043 treated tumors. Phospho-Met is associated with the host vasculature (mCD31), the cancer cells, or the stromal cells (DAPI). Scale bars represent 200 μm . Data (a) are reported as mean \pm s.e.m. Original gel images of data (b) are presented in Supplementary Fig. S6 online



HUVEC	Analysed area	Nb nodes	Nb Junctions	Nb segments	Nb branches	Tot. lenght	Tot. branching lenght	Tot. segments lenght
control(1)	144184	22	7	8	5	1075	1047	505
SP2043(1)	123840	15	3	3	4	640	360	100
control(2)	144184	55	17	22	7	1129	1129	790
SP2043(2)	138908	17	6	7	5	1064	1035	487
control(3)	163584	36	9	7	15	2096	1611	299
SP2043(3)	156240	30	8	6	13	1398	1263	430

Figure S8: Tube formation analysis

Tube formation was analyzed by using Angiogenesis Analyzer for ImageJ (NIH). The original images (left side, three images per group) were transformed to the binary images and the images were treated with the “fill hole” method: this minimizes the shadow effects in the image for the quantification. Then the images were skeletonized

(right side). The binary tree was analyzed and all the values were normalized with the analyzed area, making the area pixel number is 100,000. Among several categories of quantification, we chose number of nodes (Nb nodes), Nb junctions, Nb segments, Nb branches. Also we considered length values, including total length (Tot length), Tot branching length, and Tot segment length. From the analysis, we showed that SP2043 treatment inhibits HUVEC tube formation. Summary was plotted in Fig. 1e.